OPTICAL GAIN AND AMPLIFIED SPONTANEOUS EMISSION IN LEAD SALT SEMICONDUCTOR THIN FILM WAVEGUIDES

OPTICAL GAIN AND AMPLIFIED SPONTANEOUS EMISSION IN LEAD SALT SEMICONDUCTOR THIN FILM WAVEGUIDES

By

TIN–YU WANG, B. Eng.

A Thesis

Submitted to the School of Graduate Studies

In Partial Fulfillment of the Requirements

for the Degree

Master of Engineering

McMaster University

April 1988

MASTER OF ENGINEERING (1988) McMaster University

(Engineering Physics) Hamilton, Ontario

Canada

TITLE : Optical Gain and Amplified Spontaneous Emission in Lead Salt Semiconductor Thin Film Waveguides

AUTHOR : Tin–Yu Wang, B. Eng. (McMaster University)

Supervisors : Professor B. K. Garside

and Associate Professor P. E. Jessop

NUMBER OF PAGES :ix, 62

Abstract

The work described in this thesis involves the measurements of the optical gain and amplified spontaneous emission (A.S.E) spectrum of $Pb_{1-x}Sn_xTe$ epilayers and the establishment of conditions under which optically pumped $Pb_{1-x}Sn_xTe$ laser using a CO_2 laser as pump source can be produced.

$Pb_{1-x}Sn_xTe$ epilayers have been grown by a hot wall epitaxy (HWE) technique on BaF_2 single crystal substrates and the optical gain which can be produced in these layers has been measured by pumping the films transversely with a N_2 laser. A model for optical gain and stimulated emission as a function of pump intensity has been developed which has permitted for the first time in these materials, a direct comparison between the magnitude of the gain pumping rate, and the optical gain generated. The measured optical gain is in very good agreement with the model predicted gain. Good fits to the measured stimulated emission spectra were also obtained from the model prediction. It is shown that the gain for a given pump wavelength has a drastic dependence on the material doping density. According to the model, CO_2 laser optically pumped $Pb_{1-x}Sn_xTe$ laser can be readily achieved, provided that epilayer doping densities can be reduced to values of 10^{17} cm^{-3} or less. Nevertheless, doping densities even in nominally undoped layers are generally at least an order of magnitude too high. In some initial attempts to achieve lower doping densities, using a thermal annealing technique, doping densities as low as 2×10^{17} cm^{-3} have been obtained and significant pump absorption was achieved at CO_2 laser wavelength, as predicted by the model.

ACKNOWLEDGEMENTS

I would like to express my deep appreciation to my supervisors for their encouragement and support throughout this work. Special thanks are also due to Mr. Y. Yang for his work in growing all the epilayer films that were used in the experiments. I would also like to thank my parents for their love for me.

I also would like to express my thankfulness to my best friend, my counsellor, my motivator, my help, and my Lord, Jesus Christ.

TABLE OF CONTENTS

LIST OF FIGURES

CHAPTER 1

INTRODUCTION

1.1 General Review

The narrow band gap IV–VI semiconductors such as $Pb_{1-x}Sn_xTe$, $Pb_{1-x}S_xSe$, and $Pb_{1-x}Sn_xSe$ have long been recognized as materials which are capable of producing wavelength tunable laser action. [1] Wavelengths ranging from 3 to 30 μm can be obtained from these materials by varying the temperature and alloy composition. Fig. 1–1 illustrates the composition tuning range of some IV–VI lead salt alloys and the optical absorption peaks of some very common gas moleculesthat. This wavelength tunability makes lead salt semiconductor lasers very useful in high resolution spectroscopy, large scale ambient pollution monitoring, high sensitivity analysis of trace gases in gas mixture and heterodyne detection.[1]

Nevertheless, lead salt lasers have not yet been used widely in the industrial environment. This is mainly due to the need to operate them at cryogenic temperatures. The restricted operating temperature range of lead salt injection lasers arises from the thermal heating of the series resistance of the contacts. In homostructure diodes, very high doping density is needed to produce the required inverted population. As a result high free carrier absorption of the stimulated emission degrades the laser performance. This problem can be eliminated by using heterostructures to reduce the high free carrier density requirement. However, it is very difficult to control the doping density in the active region due to the

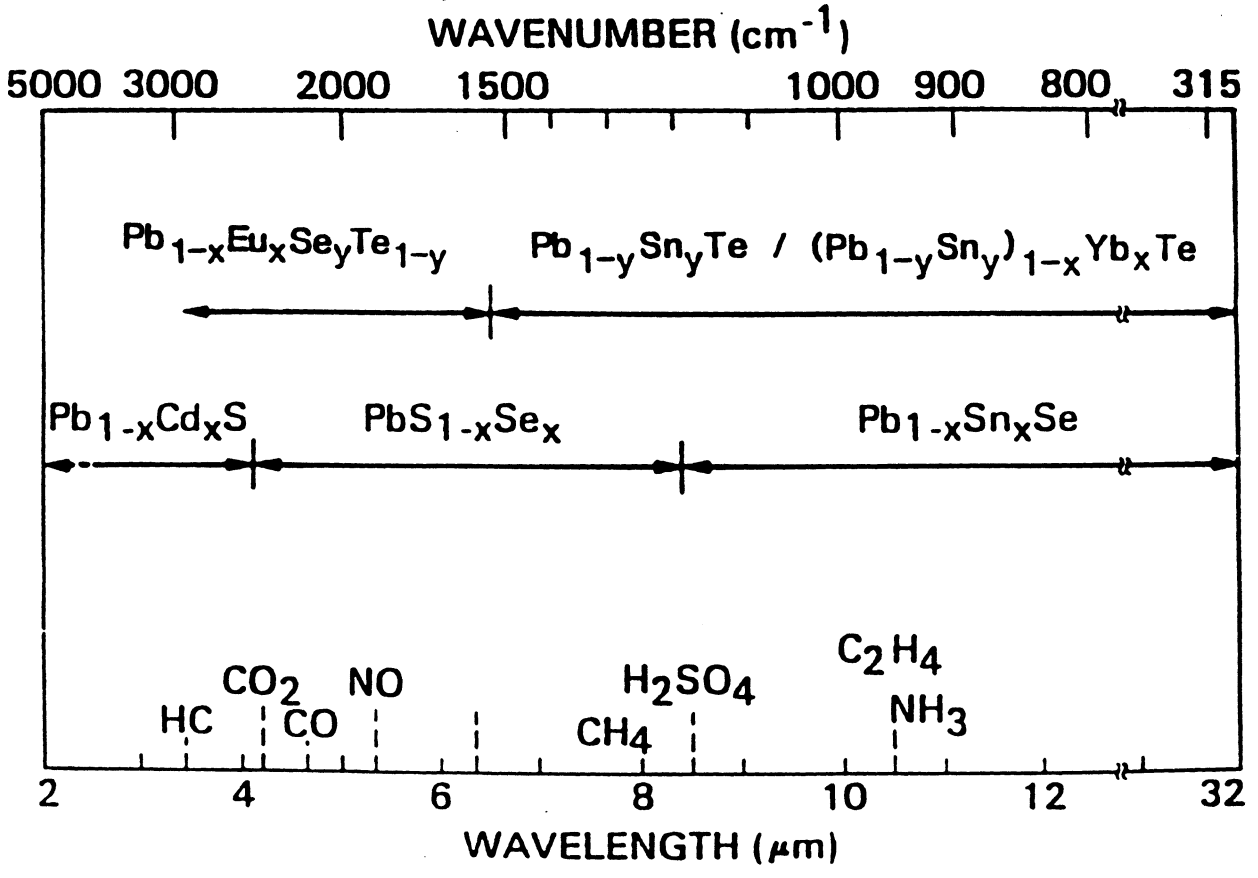

Fig.1–1 Composition tuning range of the common tenary alloys, Ref(17)

interdiffusion of Sn in these materials.[2]

Optically pumped lasers have the intrinsic advantage of needing no contacts. Thus the ohmic heating limitation of a diode laser is eliminated. Since only a single thin layer structure is required for optical pumping, the device fabrication process can be greatly simplified. Optically pumped lasers also allow the use of single crystalline insulators such as BaF_2, KCl and NaCl as substrates, and hence no interdiffusion of dopants from the substrate or other layers is possible. Moreover, single mode continuously tunable narrow linewidth optically pumped laser output can be produced at a fixed temperature, in a manner similar to a dye laser, by employing an external cavity and a diffraction grating.

A major goal of the work involved in this thesis is to investigate the possibility of producing a CO_2 laser optically pumped $Pb_{1-x}Sn_xTe$ laser. The CO_2 laser was chosen because it is the most efficient high power mid infrared laser system and it emits at wavelengths that are very close to the band gap wavelength values of $Pb_{1-x}Sn_xTe$ semiconductors.

The initial steps aimed at an optically pumped $Pb_{1-x}Sn_xTe$ laser included the exploration of the required epilayer characteristics and a determination of the pump intensity needed to generate sufficient optical gain by producing an appropriate theoretical model. Photoluminescence and gain measurement techniques were employed to establish the pump intensities required to produce laser action. Experimental results were compared to model predictions directly.

1.1.1 Photoluminescence Technique

Photoluminescence (P.L.) [3] is a process that takes place when a photon is absorbed in semiconductor materials, creating an electron–hole pair which then recombines, emitting another photon. The photon that is emitted possesses an energy that is generally very close to the semiconductor energy gap; therefore, this process can be used as a probe for the band gap of that semiconductor. In general, the photon energy of the pump source ought to be larger than the semiconductor band gap energy; often times, it can even be very close to the band gap energy. This is why optical pumping can have very high quantum efficiency. The P. L. spectrum also contains information of the energy band shape of the semiconductor material.

A photoluminescence technique was applied in this work to detect the emission intensity and spectrum, in order to make comparisons with the model predictions.

1.1.2 Gain meaurement technique

Optical gain has long been recognized as an important parameter in evaluating the possible utility of laser systems. Moreover, knowledge of the properties of the gain spectrum as a function of the pump intensity can lead to an understanding of the physics of the gain process, which in turn, can suggest ways of improving laser operating characteristics.

The gain measurement technique, which makes use of the stimulated emission, was applied in this work. [4] Fig.1–2. shows a semiconductor being excited

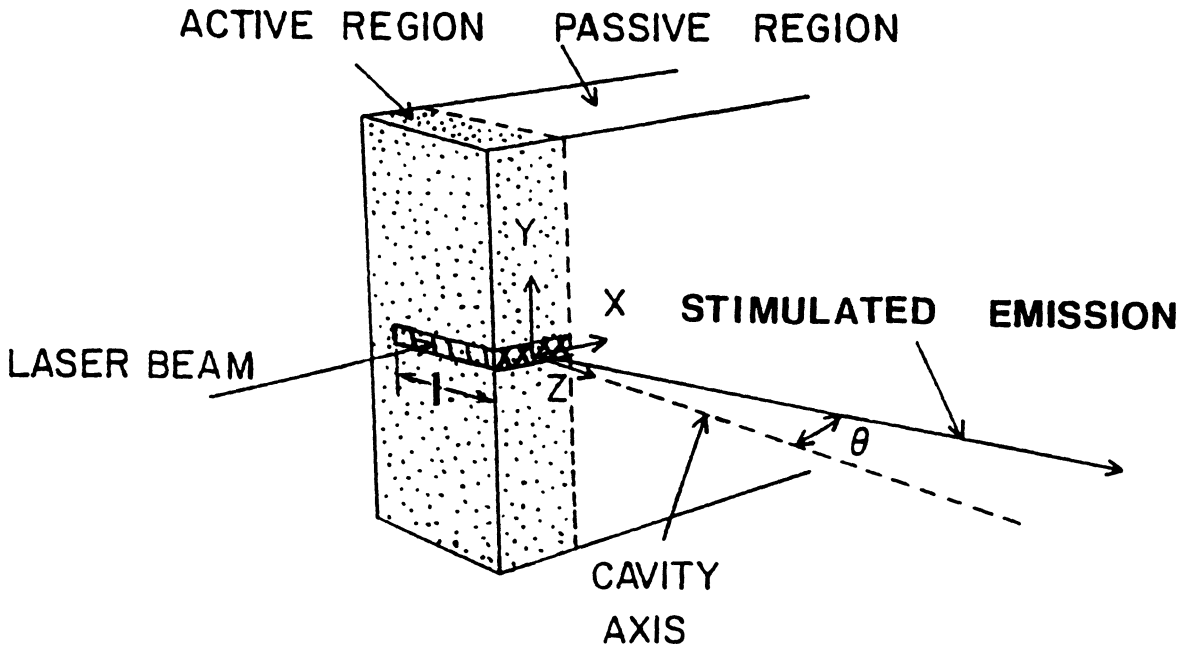

Fig.1–2 Schematic of excitation geometry for stimulated emission measurements

by a beam from a pump source at the left. It is shown that the intensity of the amplified spontaneous emission passing out the end of an excited region of length l is given by [4]

$$I\ (\text{watts–cm}^{-2}\text{–steradian}) = \frac{J_s\ \Omega}{2\ g}(e^{gl}-1)\ Tr \qquad (1.1)$$

where J_s is the spontaneous emission intensity (watts–cm^{-3}), Ω is the solid angle into which the spontaneous emission was emitted, g is the optical gain coefficient, Tr is the fraction of light that was transmitted from the semiconductor to the air. There is a factor 1/2 in eq.(1.1) because only half of the emission travels towards the direction of the cleaved surface.

A plot of intensity as a function of the length of the excited region according to eq.(1.1) is given in fig.1–3 for different values of the gain parameter g. By manipulating eq.(1.1), we can calculate gain

$$g = \frac{\ln(I) - \ln(I')}{l - l'} \qquad (1.2)$$

I and I' are the corresponding emission intensities for pump stripe lengths l and l' respectively. This equation is valid as long as the emission intensity, I, increases exponentially with the pump stripe length, l. This corresponds to a e^{gl} value which is greater than 2 but less than 10 in general. When e^{gl} is less than 2, spontaneous emission dominates. When e^{gl} is greater than 10, the optical gain reaches saturation, and thus the emission intensity no longer increases exponentially

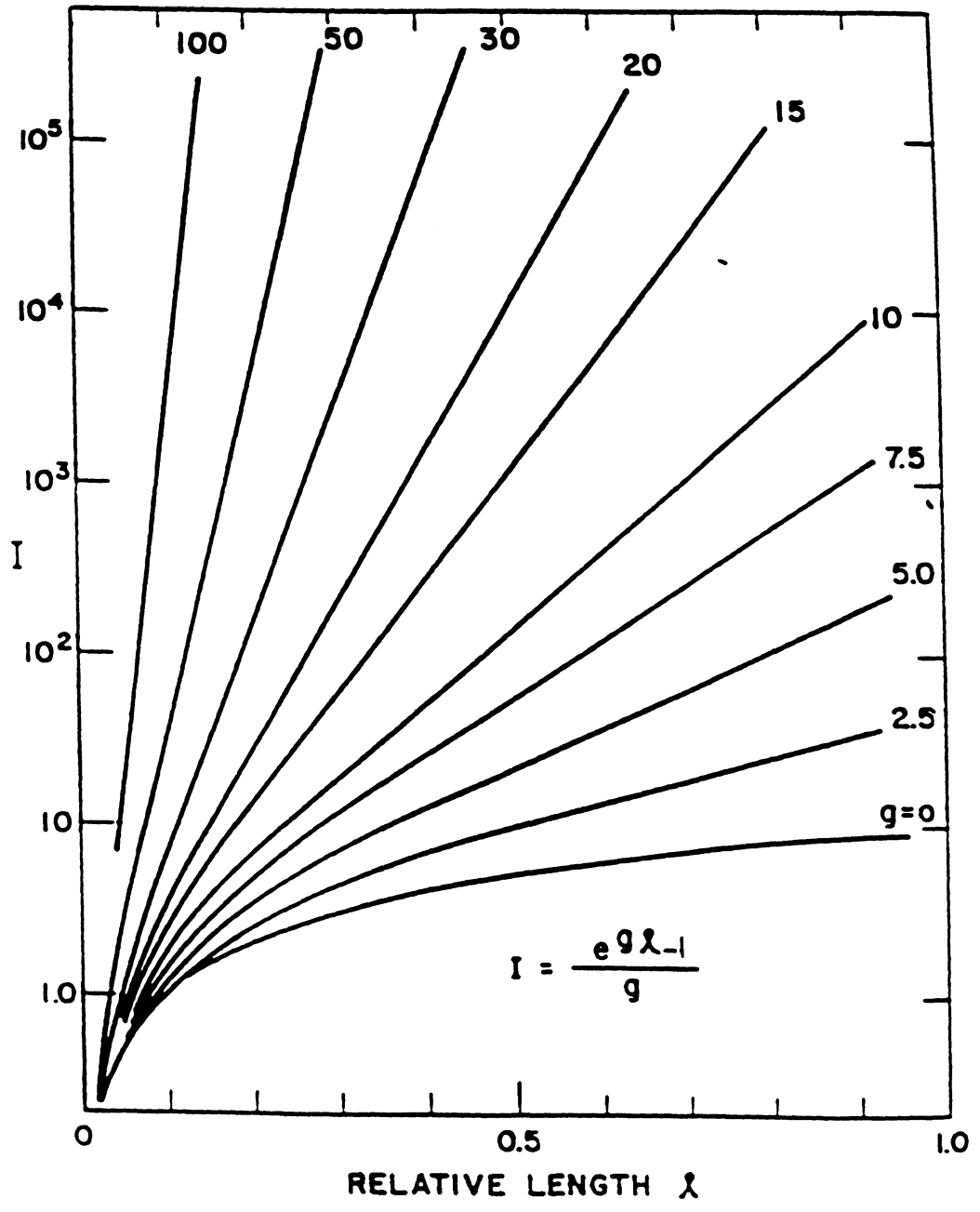

Fig.1–3 Expected variation of the amplified luminensence intensity with excitation length for different values of the gain, Ref(4)

with the pump stripe length. When e^{gl} is less than 10 but greater than 2, stimulated emission dominates and the intensity increases exponentially with the pump stripe length. Therefore, we can obtain the gain coefficient by calculating the slope of the linear region of the emission intensity vs. stripe length curve in fig. 1–3.

1.1.3 Film Preparation

All the $Pn_{1-x}Sn_xTe$ films that were used for optical pumping experiments were grown by Mr. Y. F. Yang using the hot wall epitaxy system (HWE) at McMaster.

Hot wall epitaxy is a vacuum film deposition technique whose main characteristic is the growth of epitaxial layers under conditions as near as possible to thermodynamic equilibrium and with a minimum loss of material.[5] The main feature of HWE is the use of a heated–liner (hot wall) which serves to enclose and direct the vapor from the source to the substrate. Fig.1–4 shows a simplified schematic diagram of a hot wall system. There are three advantages of this technique. The loss of evaporating material is avoided, the vapor pressure of the compound can be maintained, and the difference between the substrate and source temperature can be reduced to a minimum.

The films were epitaxially grown on cleaved surfaces along <111> direction of BaF_2 single crystal substrates at a temperature of 250°C. The reason for growing the films at such low temperature was to reduce the doping densities of the films. As–grown films produced by hot wall epitaxy have typical p type doping densities of 10^{18} cm^{-3} to 10^{19} cm^{-3} with film thicknesses form 1 to 5 μm. This

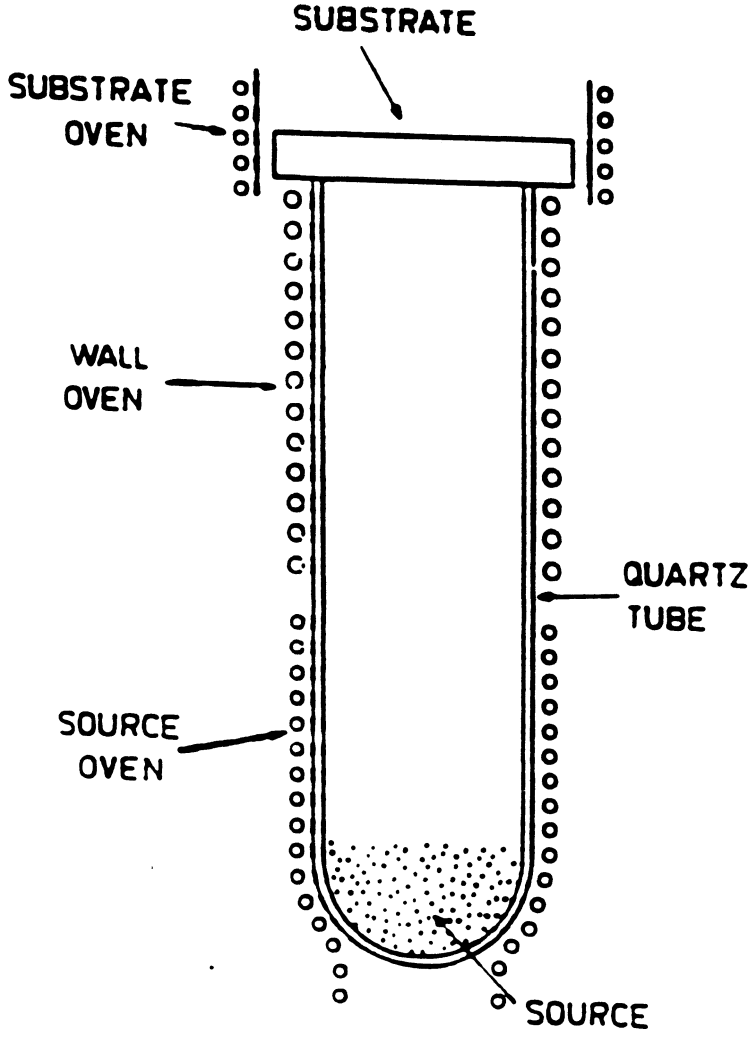

Fig.1–4 Schematic of the hot wall system, Ref(5)

high doping density is due to the high mobility of Sn which easily diffuses out of the film and leaves the film with an excess of Te. [2,5] The excess Te in the film acts as a p–type dopant which accounts for the generally high doping densities in $Pb_{1-x}Sn_xTe$ films. The as–grown films had carrier mobilities of as high as 1000 $cm^2 V^{-1}–sec^{-1}$ at room temperature as measured by Hall effect. This high carrier mobility showed that the films had a very low degree of scattering centres, which means that the as–grown material was of very high crystal quality.

Apart from good crystal quality of the film, good optical quality edge (smooth over an area of the order of the square of the emission wavelength, about 100 μm^2 in this case) perpendicular to the film surface is necessary in order to measure the single pass optical gain along the transverse direction of the film accurately. Since BaF_2 can only be cleaved along <111> direction, and the <111> surfaces are at angles of either 60^0 or 120^0 to the other <111> surfaces, cleaved edges that are perpendicular to the film surface cannot be obtained. Moreover, $Pb_{1-x}Sn_xTe$ can only be cleaved along the <100> directions. Therefore, cleaved edges, that are perpendicular to the film surface, can only be obtained from epilayers that are grown on subatrates that have cleavage planes along the <100> directions, such as NaCl anb KCl. Mechanical polishing techniques were used to polish the samples along the direction that is perpendicular to the film surface to make smooth edges. The polished film surfaces and edges were observed under optical microscope and found to be of high optical quality.

1.2. Outline of the Contents of the thesis

Chapter two begins by presenting a gain model originally proposed by Anderson. [6] The capabilities and accuracy of the model are discussed. A cw laser pumping model which calculates the optical gain and stimulated emission spectra with respect to the pump intensity is described. The capabilities of the model and some model predictions are also discussed. The full expression of the real part of the dielectric constant is presented and discussed. The significance of the contribution to the dielectric constant from each individual term is considered. Results of optical transmission of films with various doping densities are also compared with the model predictions. The possibility of a CO_2 laser optically pumped $Pb_{1-x}Sn_xTe$ laser and the required film characteristics are then discussed according to the model predictions.

Chapter three presents a pulsed laser pumping model which calculates the dependence of the optical gain and stimulated emission spectra on pump intensity in non steady state conditions and the results from the N_2 laser optical pumping experiments. A N_2 laser was chosen as the pump source since the optical absorption of $Pb_{1-x}Sn_xTe$ films remains very high at short wavelengths, even at very high doping densities. The presence of gain and loss regions within the epilayer was shown to be caused by the very high optical absorption effect at N_2 laser wavelength (.337 μm). Result of the predicted complex dielectric constant spatial distribution is presented and the need of a complex waveguide model is also discussed. A step index complex dielectric profile waveguide model is used to approximate the size of the waveguide modes. Experimental results of the

mode–gain and emission spectra are compared with the model predictions. Finally, the appropriateness of the model is evaluated.

Chapter four summarized the results discussed in the previous two chapters. Conclusions and further research suggestions are presented.

CHAPTER 2

CO_2 LASER OPTICAL PUMPING

2.1 Introduction

A cw laser pumping model is presented in this chapter to calculate the gain and stimulated emission spectra with respect to CO_2 laser pump intensity. There are two optical gain models for $Pb_{1-x}Sn_xTe$ [6,7], which have been suggested by different authors. The one that was suggested by Grisar et al [7] uses a parabolic band approximation, which is very simple mathematically, but does not describe the energy bands of $Pb_{1-x}Sn_xTe$ very accurately. The model we have chosen for this calculation was Anderson's gain model [6] which uses an asymmetric band model and assumes k selection rule for carrier transitions. The asymmetric band parameters that Anderson used in his gain model were from Hewes et al [8] and had been shown to provide remarkable agreement with experimental data over a wide range of sample compositions, temperatures and carrier concentrations. [8] The band parameters and magnetic hyperfine constants were experimentally determined by nuclear magnetic resonance study. k selection rule forces the carrier momentum to be conserved for carrier transitions. The optical absorption spectrum predicted by Anderson's band model accurately reproduced the published absorption spectrum of PbTe [9] and can be taken as partial vindication of the use of the k–conservation selection rule.

The complete model for CO_2 laser optical pumping is described in section 2.2.

2.2 CO2 Laser Optical Pumping Model

Before going into the details of the CO_2 laser optical pumping model, Anderson's gain–frequency model is briefly described here. Firstly, Anderson uses an asymmetric band model to describe the energy band shape. [10] The E–k dispersion relationship is given by [10]

$$\left[E_g - E + \frac{\hbar^2}{2m_o}\left(\frac{m_o}{m_t^-}k_t^2 + \frac{m_o}{m_l^-}k_l^2\right)\right]\left[E + \frac{\hbar^2}{2m_o}\left(\frac{m_o}{m_t^+}k_t^2 + \frac{m_o}{m_l^+}k_l^2\right)\right] + P_t^2k_t^2 + P_l^2k_l^2 = 0 \qquad (2.1)$$

in which the energy band gap is given by [2]

$$E_g = 171.5 - 535x + \sqrt{(12.8)^2 + .19(T+20)^2} \qquad (2.2)$$

and this energy band gap expression is established by a calculated fit to low temperature energy band gap data [1], and the the matrix element values are

$$P_t = 4.61 \times 10^{-8}\ \text{eV–cm} \qquad P_l = 1.40 \times 10^{-8}\ \text{eV}$$

$$\frac{m_o}{m_t^+} = 10.36 \qquad \frac{m_o}{m_l^+} = 0.75$$

$$\frac{m_o}{m_t^-} = 11.60 \qquad \frac{m_o}{m_l^-} = 1.20$$

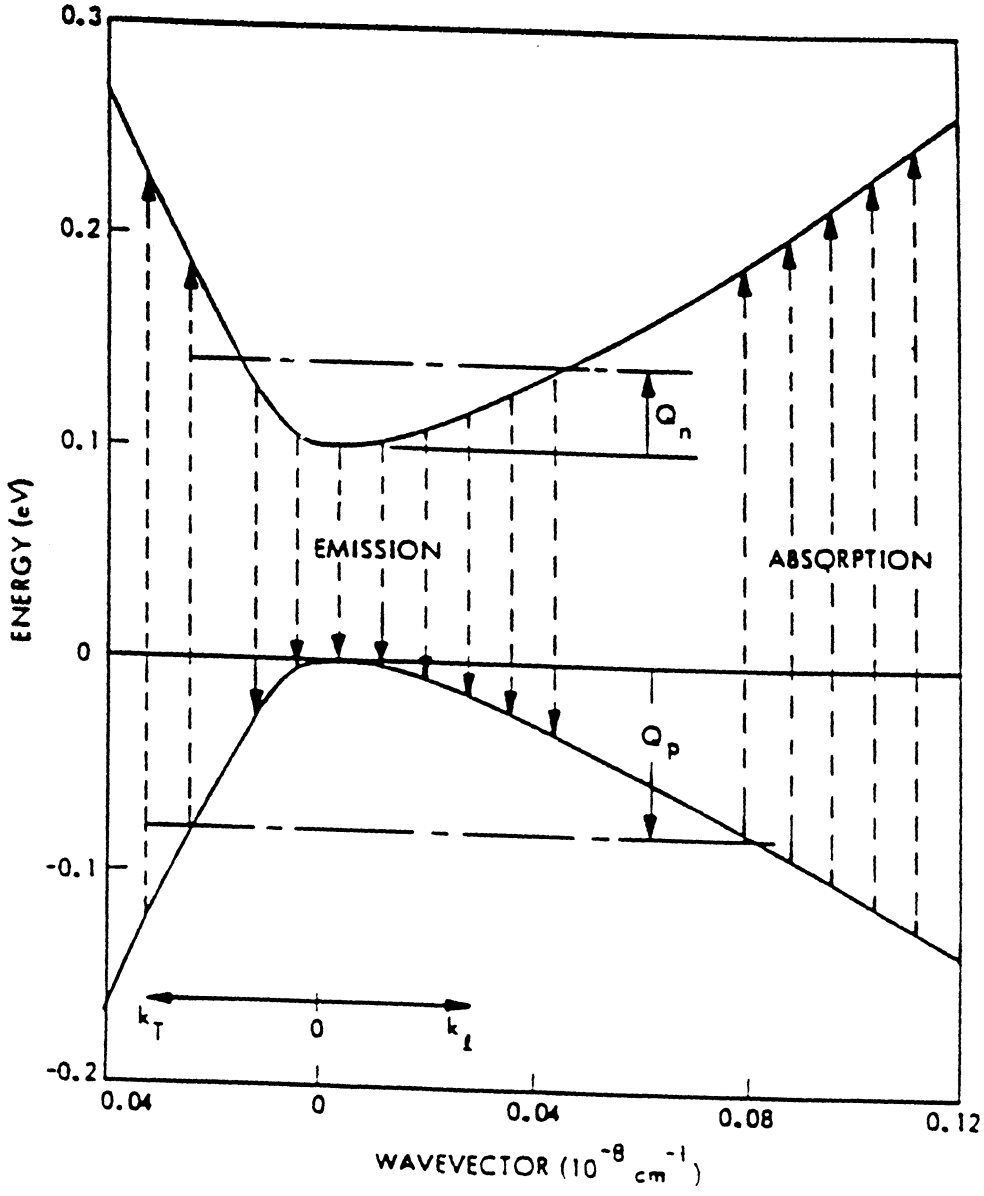

Fig.2–1 E–k relationship of the energy bands of $Pb_{1-x}Sn_xTe$ at T ≃ 0K, Ref(6)

and these parameters were from nuclear magnetic resonance study done by Hewes et al [8] as discussed in the previous section.

Fig.2–1 illustrates the asymmetric band structure, where the E–k relation is shown both along the longitudinal and the transverse k directions. The transverse and longitudinal k vectors are defined by the directions that are perpendicular and parallel to the (1,1,1) axis at the L point of the Brillouin zone in the k space. One can observe that the conduction band and the valence band shapes are highly asymmetrical.

With the band parameters known, it is possible to calculate the quasi fermi levels with respect to the bands relating to the electron and hole densities.

$$N = N_c f_u \tag{2.3}$$

$$P = N_v f_l \tag{2.4}$$

N_c and N_v are the density of states in the conduction band and density of states in the valence band respectively. f_u and f_l are the quasi–fermi integrals for the conduction and valence bands respectively. Fermi integrals are statistical functions that are used to describe the free carrier distributions within the energy bands. The value of the fermi integral is a function of the position of the fermi levels with respect to the conduction band and valence band edges. The fermi integral for the conduction band is related to the quasi fermi level with respect to the conduction band and the fermi integral for the valence band is related to the quasi–fermi level with respect to the valence band.

$$f_u = F_{.5}\left(\frac{Q_n}{kT}\right) \tag{2.5}$$

$$f_l = F_{.5}\left(\frac{Q_p}{kT}\right) \tag{2.6}$$

where k is the Boltzman constant and T is the temperature. Q_n and Q_p are given by

$$Q_n = f_u - E_c \tag{2.7}$$

$$Q_p = E_v - f_l \tag{2.8}$$

where E_c and E_v are the bottom of the conduction band and the top of the valence band respectively. f_u and f_l are the quasi fermi levels for electrons and holes. The density of states is given by [6]

$$Nc = \frac{\left[\frac{E_g kT}{\pi}\right]^{3/2}}{\left[Eg\frac{\hbar^2}{2m_o}\frac{m_o}{m_t^-} + P_t^2\right]\left[Eg\frac{\hbar^2}{2m_o}\frac{m_o}{m_l^-} + P_l^2\right]^{1/2}} \tag{2.9}$$

$$Nv = \frac{\left[\frac{E_g kT}{\pi}\right]^{3/2}}{\left[Eg\frac{\hbar^2}{2m_o}\frac{m_o}{m_t^+} + P_t^2\right]\left[Eg\frac{\hbar^2}{2m_o}\frac{m_o}{m_t^+} + P_l^2\right]^{1/2}} \tag{2.10}$$

Nc and Nv are the conduction band density of states and the valence band density of states respectively. Since the Fermi Integral can not be solved analytically, we use an approximation method given by Blakemore [11]

$$F_{.5}\left(\frac{Qn}{kT}\right) = \frac{.886}{0.27+\exp\left(-\frac{Qn}{kT}\right)}, \quad \frac{Qn}{kT} < 1 \tag{2.11}$$

$$F_{.5}\left(\frac{Qn}{kT}\right) = .667\left(\left(\frac{Qn}{kT}\right)^2+1.645\right)^{3/4}, \quad \frac{Qn}{kT} > 1 \tag{2.12}$$

It has been shown that the above approximations reproduce the fermi integral values accurately. [11]

The gain model for Pb salt materials is a k–conserved calculation; unlike the III–V semiconductors such as GaAs, which does not obey the k–selection rule at very high doping densities. [12] According to Anderson, the gain expression is given by

$$g = \frac{8\left(\frac{1}{3}P_l^2+\frac{2}{3}P_t^2\right)\left[\left(1-\exp\left(\frac{\hbar\omega-Eg-Qn-Qp}{kT}\right)\right)\right]}{137\sqrt{\epsilon_\infty}\,\hbar\omega\left[1+\exp\left(\frac{\hbar\omega-Eg-2Qn}{2kT}\right)\right]\left[1+\exp\left(\frac{\hbar\omega-Eg-2Qp}{2kT}\right)\right]}$$

$$\cdot\frac{\left(\frac{\hbar\omega+Eg}{2}\right)\sqrt{\hbar\omega-Eg}}{\left[Eg\frac{\hbar^2}{2m}\left(\frac{m_o}{m_t^-}+\frac{m_o}{m_t^+}\right)+2P_t^2\right]\left[Eg\frac{\hbar^2}{2m}\left(\frac{m_o}{m_l^-}+\frac{m_o}{m_l^+}\right)+2P_l^2\right]^{1/2}} \tag{2.13}$$

We can calculate the gain/absorption spectrum with the knowledge of

the band gap, temperature, and doping density. The terms which involve Qn and Qp, represent the Moss–Burstein effect [13,14] of the optical absorption edge shift. This optical absorption edge shift is caused by the emptying of the bound states in the valence band or the filling up of the free states of the conduction bands by introducing high free carrier densities. The free carrier density can be increased by enhancing either the background doping or the non–equilibrium excitation of free carriers. This free carrier density turns out to be a very important effect in varying the absorption coefficient of the material.

With the knowledge of the gain–frequency spectrum for specific free carrier density, we can proceed to describe the method to relate optical pump intensity to gain/absorption spectrum.

When the epilayers are excited by the laser power, the quasi–fermi levels are separated by a certain amount of energy, which varies with the level of excitation. This energy is

$$u = f_u - f_l \tag{2.14}$$

From (eq.2.14) we can rewrite it as

$$u - Eg = Q_n + Q_p \tag{2.15}$$

where Q_n and Q_p are the quasi–fermi levels measured from the conduction and valence bands respectively.

To start the calculation, we assume a certain separation of the quasi–fermi levels, u; and we proceed to evaluate the corresponding spontaneous

emission rate. Spontaneous emission rate is given by [12]

$$r_{spon}(E) = \frac{4\pi\epsilon_o n^2 E^2}{\pi^2 c^2 \hbar^2} g(E) \frac{f_u(1 - f_l)}{f_u - f_l} \tag{2.16}$$

Where g(E) is the gain spectrum according to eq.(2.13); n is the refractive index of the material.

From the spontaneous emission spectrum $r_{spon}(E)$, we can calculate the total spontaneous emission rate, which is equivalent to the spontaneous recombination rate.

$$R_{spon} = \int_0^\infty r_{spon}(E)\, dE \tag{2.17}$$

As we can see from eq.(2.17), the spontaneous emission spectrum extents to very high energy levels inside the band. However, due to the Fermi distribution of free carriers, the deeper into the energy bands, the less likely it is for free carriers to be present. Therefore, $r_{spon}(E)$ is expected to be a rapidly decaying function of energy, E. In our calculations, we've chosen appropriate energy levels by continuously checking the R_{spon} value as the numerical integration proceeds and stop the calculation when the R_{spon} value converges to a predetermined accuracy.

For steady state conditions, the recombination rate R equals the generation rate of free carriers

$$G = R \tag{2.18}$$

other recombination processes that are non–radiative are accounted for by assuming a quantum efficiency. We assume a quantum efficiency η to define the fraction of recombinations that occurred radiatively

$$G = \frac{R_{spon}}{\eta} \tag{2.19}$$

Now, we can predict the pump intensity required to produce a particular generation rate

$$I_o = \frac{R_{spon}^{*} \quad th}{Tr \ (1 \ - \exp(-\alpha^{*}th)) \ \eta} \tag{2.20}$$

where I_o is the required pump intensity

th is the film thickness

Tr is the air–film interface optical transmission

α is the absorption coefficient at the pump wavelength for a particular pump intensity

Notice here that it is essential to choose Tr and not 1 – Re (Re is the air–film interface reflection), since light travels slower in the film than in the air due to the change of refractive index. This in turn alters the pump intensity I_o by a factor of n.

From eq.2.20, we can see that all the parameters are known except the refractive index term involved in the total spontaneous recombination rate, R_{spon} and the optical transmission, Tr.

In order to calculate the refractive index, we have to consider each individual term that contributes to the dielectric constant. The dielectric constant is based on the well known expression. [15]

$$\epsilon = \epsilon_\infty + \Delta\epsilon(\lambda) - (Ne^2/4\pi c^2 m_c^- \epsilon_o)\lambda^2 - (Pe^2/4\pi c^2 m_c^+ \epsilon_o)\lambda^2$$

$$- \epsilon_\infty(1 - \epsilon_\infty/\epsilon_s)(\lambda/\lambda_{Lo})^2 \qquad (2.21)$$

ϵ_s is the static dielectric constant. ϵ_∞ is the contribution to the dielectric constant due to the bound carriers. $\Delta\epsilon(\lambda)$ is the the contribution to the dielectric constant from regions close to the absorption edge. The third and fourth terms are the contribution arising from the free carrier effect. N and P are free carrier densities of electrons and holes. m_c^- and m_c^+ are the conductivity effective mass of the conduction and valence bands respectively. The last term represents contribution due to optical phonons with wavelength λ_{Lo}.

In our calculations, we have employed Gopal's empirical formula [16], which is in good agreement with the experimental results of the dielectric constant.

$$\epsilon_\infty = 1 + \frac{C}{(Eg + D)^2} \qquad (2.22)$$

where C = 74.82 and D = 1.21 for $Pb_{1-x}Sn_xTe$. The calculated ϵ_∞ from this expression gives values that are comparable to the experimental values with an accuracy of about 15%.

$\Delta\epsilon(\lambda)$ represents the dispersion of the index of refraction. [15]

$$n(E)-1 = \frac{\hbar c}{2\pi E}\int_0^\infty [d\alpha(E')/dE'] \ln[(E'+E)/(E'-E)]\, dE' \qquad (2.23)$$

where n(E) is the refractive index at photon energy, E, and $\alpha(E')$ is the optical absorption coefficient at photon energy, E'.

It was found that the change of refractive index, Δn at its peak is about 0.5 and is almost independent of carrier density. [15] Since the major confinement mechanism in this material is due to the change of free carrier density, the effect of this term to the change of the refractive index is rather small. Therefore, this term does not contribute much to the change of the waveguide confinement factor and can be neglected.

It was found that the contribution of the lattice dispersion is about 0.1 at $\lambda = 10\ \mu m$. [15] Since the term is very small and almost independent of temperature and carrier concentration, it was neglected.

The free carrier contribution to the dielectric constant was calculated using Anderson's band parameters for the conductivity effective mass. [6] Due to the small value of the conductivity effective mass of $Pb_{1-x}Sn_xTe$, the contribution of the free carrier term becomes comparable to ϵ_∞ for high carrier concentration and long wavelengths.

Therefore, we simplified eq.(2.21) in our calculations.

$$\epsilon = \epsilon_\infty - (Ne^2/4\pi c^2 m_c^- \epsilon_0)\lambda^2 - (Pe^2/4\pi c^2 m_c^+ \epsilon_0)\lambda^2 \qquad (2.24)$$

Unfortunately, there is insufficient experimental data of the refractive

index with respect to the film doping density available to determine how accurately eq.(2.24) describes the free carrier effect on the dielectric constants. However, the expression for the free carrier term contribution to the dielectric constant is very well established and the effective mass values were derived from very good experimental data. Therefore, eq. (2.24) is expected to be a very accurate expression for the free carrier effect on the refractive index.

The model that we just described is capable of relating the pump intensity with the gain and amplified spontaneous emission spectra. Predictions from this model can be compared with the experimental results directly.

2.3 Model Predicted Pumping Conditions

Having established the laser pumping model, we can now proceed to predict the pumping conditions required to generate sufficient optical gain to produce laser action in $Pb_{1-x}Sn_xTe$.

The obvious question is what percentage of Sn is required in the epilayer in order to shift the optical absorption edge to long enough wavelengths to utilize a CO_2 laser as the pump source. The epilayer material has to have a band gap energy which is smaller than the CO_2 laser photon energy. In this case, the shortest wavelength laser line available in the CO_2 laser, that we employed, was the 9P(16) line, which emits at 9.52 μm. The band gap wavelength value, hence, has to be longer than the pump wavelength. Since the band gap value of $Pb_{1-x}Sn_xTe$ is also dependent on temperature according to eq.(2.2), we will look at the required percentage of Sn at both liquid N_2 (77K) and He (4.2K) temperatures. According to eq.(2.2), x (% of Sn) has to be larger than 16% at T = 77K, and 11% at T = 4.2K.

Unfortunately, the percentage of Sn in this alloy material is not the only factor that affects the effective optical absorption edge of the epilayer. It turns out that the doping density of the epilayer is a critical factor which affects the location of the optical absorption edge in the frequency space. This shifting of the optical absorption with doping density is known as the Moss–Burstein effect, which is included in eq. (2.13), the gain expression. The terms that involve the quasi–fermi levels Qn and Qp in eq. (2.13) are responsible for the shifting effect. The positions of the quasi fermi levels are determined by the free carrier density of the epilayer. The free carrier density change can be caused by the background doping density, which is a material characteristic or the density of the excited free

carriers, which are generated by the pump source (laser in this case). Therefore, the exact location of the absorption edge in the frequency space is the combined effect of the doping density of the layer and the pump intensity of the excitation source. Fig.2–2 shows the shifting of the absorption edge of a 14 % Sn, $Pb_{1-x}Sn_xTe$ film, due to changes in the doping density of the epilayer. The optical absorption coefficient at the pump wavelength, 9.52 μm, changes from about 6000 cm^{-1} to a few 10's of cm^{-1} as the doping density changes from 0.5 x 10^{17} cm^{-3} to 1.5 x 10^{17} cm^{-3} at 10K. Fig.2–3 shows the change in the optical absorption coefficient of a 18 % Sn, $Pb_{1-x}Sn_xTe$ film, at 9.52 μm from about 3000 cm^{-1} to 1000 cm^{-1} for a change of doping densities from 1 x 10^{17} cm^{-3} to 3 x 10^{17} cm^{-1} at T = 77K.

In order to get laser action, it is very important that that the films have high enough optical absorption at the pump wavelength. Optical gain coefficient of 6000 cm^{-1} in a 5 μm thick film will absorb about 90 % of the pump power. Therefore, an optical absorption coefficient of at least 6000 cm^{-1} is needed for films with thicknesses less than 5 μm so that most of the pump power will be absorbed by the film. From the model's predictions shown in figs. 2–2 and 2–3, film doping density of 10^{17} cm^{-3} or less is needed so that an absorption coefficient of 6000 cm^{-1} or more could be achieved at 9 μm CO_2 laser lines.

By comparing the change in absorption spectrum of both figs.2–2 and 2–3, we can conclude that the change in optical absorption is less at 77K than at 10K. This is because of the spreading of the allowed electron and hole states inside the energy bands caused by the icreased thermal energy. It is very important to notice that the change of the optical absorption with material doping density only occurs at pump wavelengths that are close to the material energy band gap wavelengths. Fig.2–4 shows the decrease of the value of the absorption coefficient of

Fig.2–2 Model predicted absorption wavelength spectra for 14 % Sn, $Pb_{1-x}Sn_xTe$ at T = 10k (□ P = 5 x 10^{16} cm^{-3}; + P = 1 x 10^{17} cm^{-3}; <> P = 1.5 x 10^{17} cm^{-3})

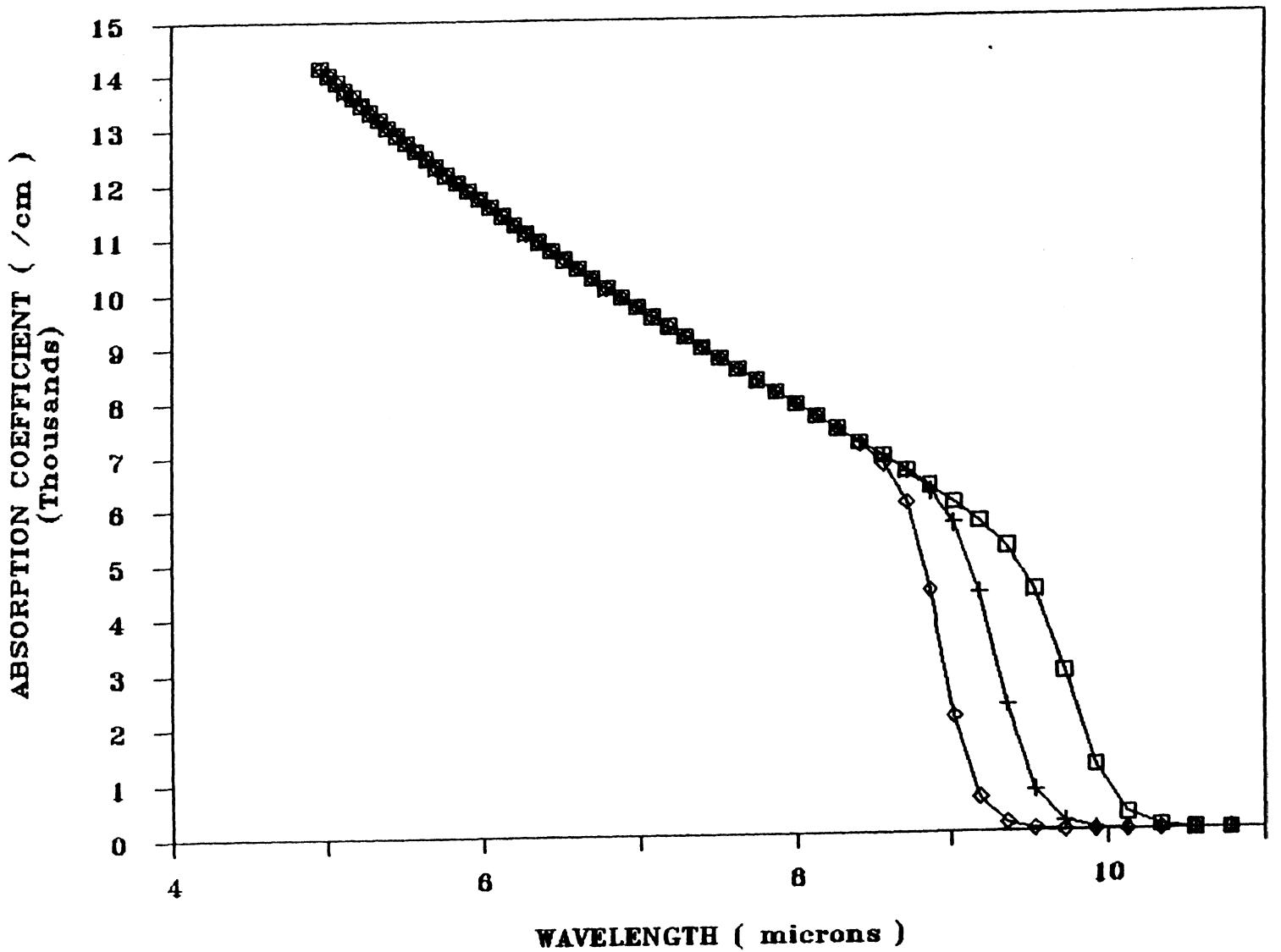
ABSORPTION COEFFICIENT (/cm)
(Thousands)
15
14
13
12
11
10
9
8
7
6
5
4
3
2
1
0
4
6
8
10
WAVELENGTH (microns)

Fig.2–3 Model predicted absorption wavelength spectra for 14 % Sn, $Pb_{1-x}Sn_xTe$ at T = 77k (□ P = 1 x10 $^{17}cm^{-3}$; + P = 2 x 10 $^{17}cm^{-3}$; <> P = 3 x 10 $^{17}cm^{-3}$)

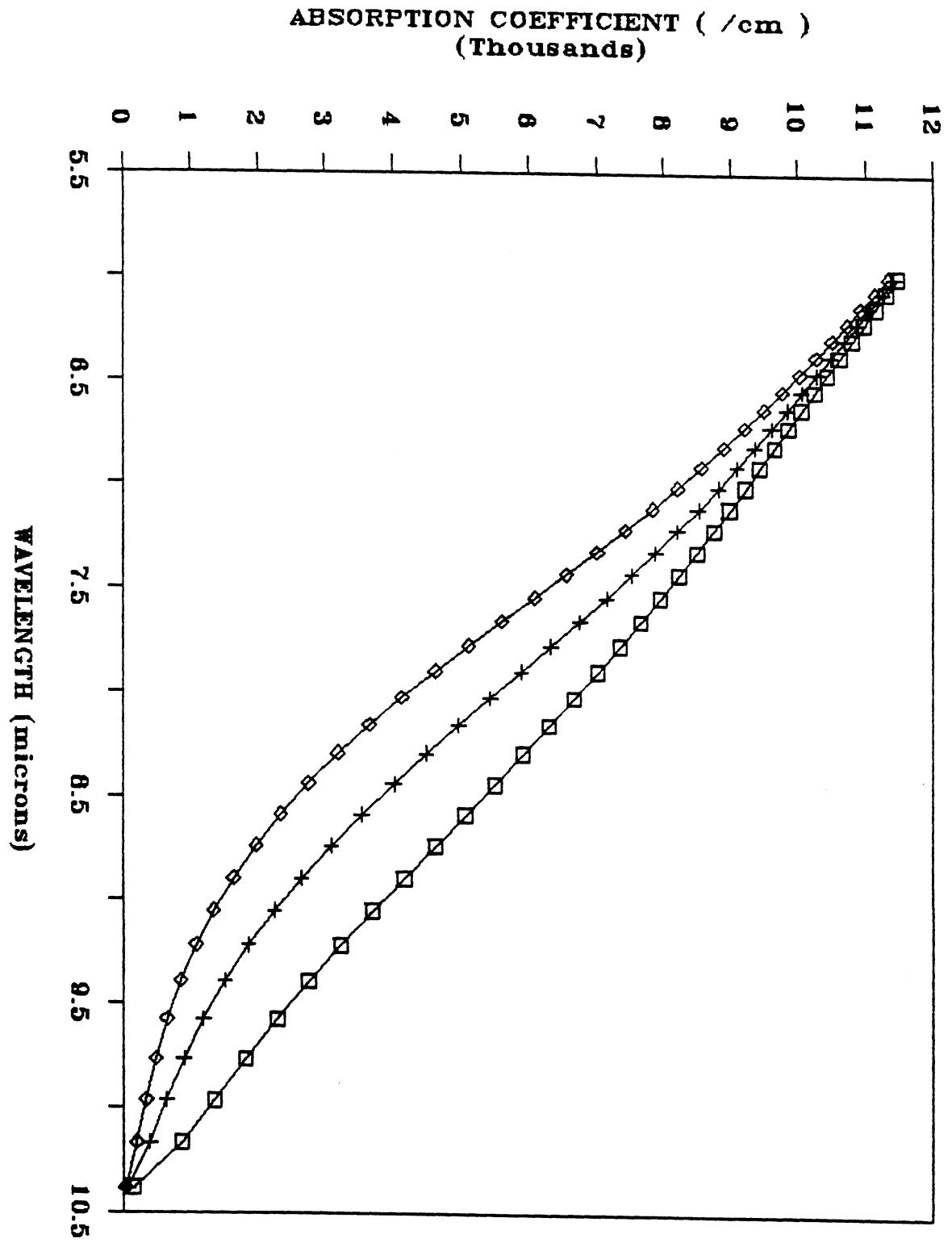
ABSORPTION COEFFICIENT (/cm)
(Thousands)
0
1
2
3
4
5
6
7
8
9
10
11
12
5.5
6.5
7.5
8.5
9.5
10.5
WAVELENGTH (microns)

Fig.2–4 Model predicted absorption wavelength spectra for 18 % Sn, $Pb_{1-x}Sn_xTe$ with P = 1 x $10^{17}cm^{-3}$ at T = 77k (□ I = 1000 Wcm^{-2}; + I = 3000 Wcm^{-2}; <> I = 5000 Wcm^{-2})

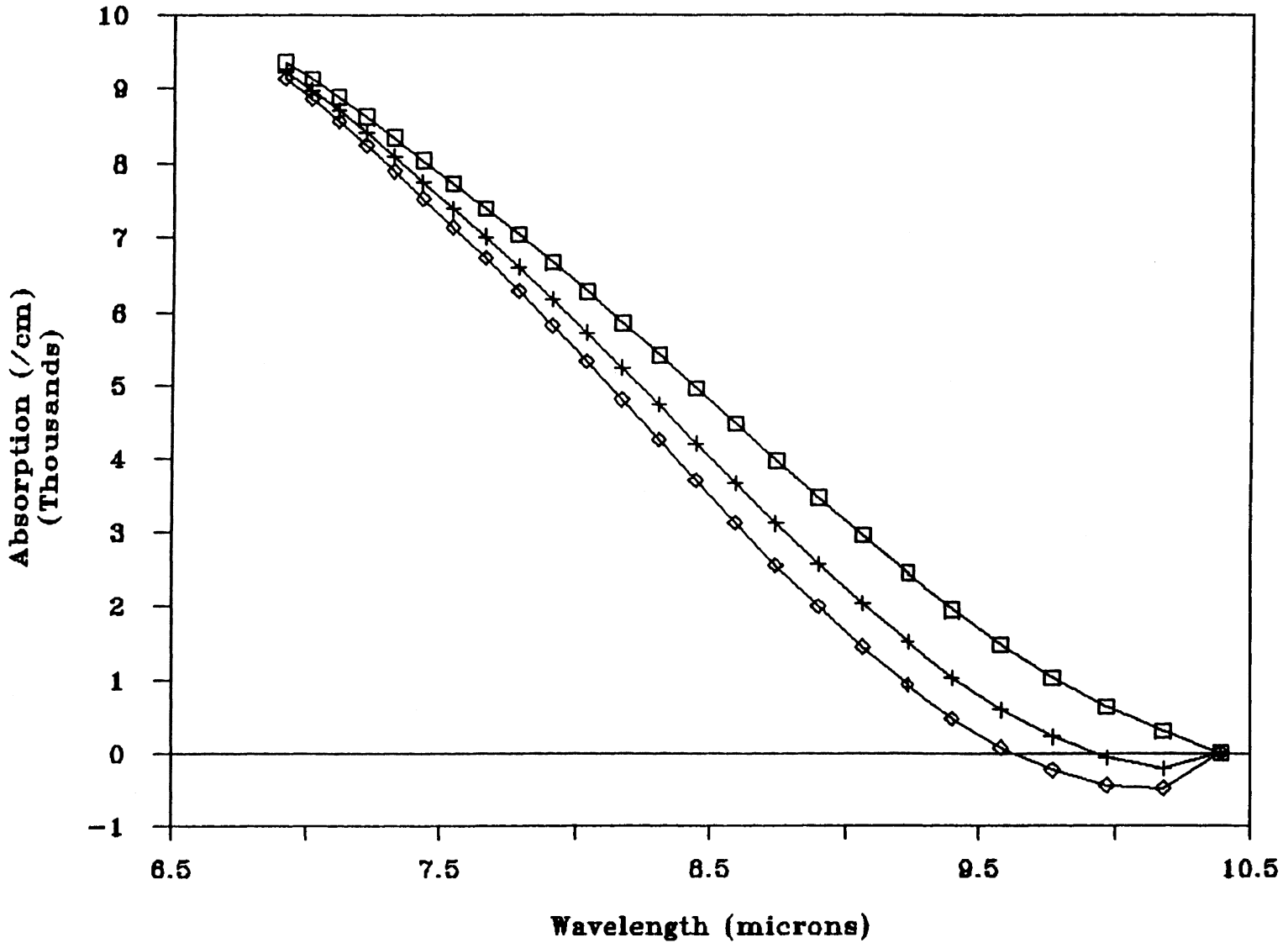
10
9
8
7
6
5
4
3
2
1
0
−1
Absorption (/cm)
(Thousands)
6.5
7.5
8.5
9.5
10.5
Wavelength (microns)

a 18 % Sn, $Pb_{1-x}Sn_xTe$ film, with p–type doping density of 10^{17} cm^{-3} at 9.52 μm from about 2000 cm^{-1} to a few 10's of cm^{-1} with pump intensity increased from 1000 W cm^{-2} to 5000 W cm^{-2}. This effect is only significant at which the wavelength of the pump source is very close to the energy band gap wavelength of the material. Therefore, by employing a shorter wavelength pump laser, the high optical absorption in the epilayer film can be maintained even at very high doping density. This is the major reason why the N_2 laser was chosen as the pump source in the experiments described in chapter three.

From the model predictions shown previously, film doping densities have to be less than 10^{17} cm^{-3} so that an optical absorption coefficient of 6000 cm^{-1} or higher can be achieved at CO_2 laser wavelengths. Let's assume that such low doping density has been obtained; what is the required pump intensity in order to produce sufficient optical gain for laser action ? This question can be answered by looking at the gain–frequency spectra for various values of pump intensity and comparing those values with the required gain. Fig.2–5 is the absorption–frequency spectrum of a 14 % Sn, $Pb_{1-x}Sn_xTe$ film at a pump wavelength of 9.52 μm for different values of pump intensity at 10K. An optical gain coefficient value of $\simeq$ 200 cm^{-1} can be achieved with very low pump intensity of about 200 Watts cm^{-2} by using a quantum efficiency value of 10%, which was calculated from the observed emission intensity of the N_2 laser pumping experiments to be described in chapter three. Fig.2–6 is the gain–frequency spectrum of a 20 % Sn, $Pb_{1-x}Sn_xTe$ film at a pump wavelength of 9.52 μm for different pump intensities at 77K. In this case, a higher pump intensity is required to produce the same amount of gain, however, the pump intensity required is still reasonably low ($\cong$ 2000 Watts cm^{-2}).

Fig.2–5 Model predicted optical gain spectra for 14 % Sn, $Pb_{1-x}Sn_xTe$ at T = 10K (□ I = 10 W cm^{-2}; + I = 50 W cm^{-2}; <> I = 100 W cm^{-2}; Δ, I = 200 W cm^{-2})

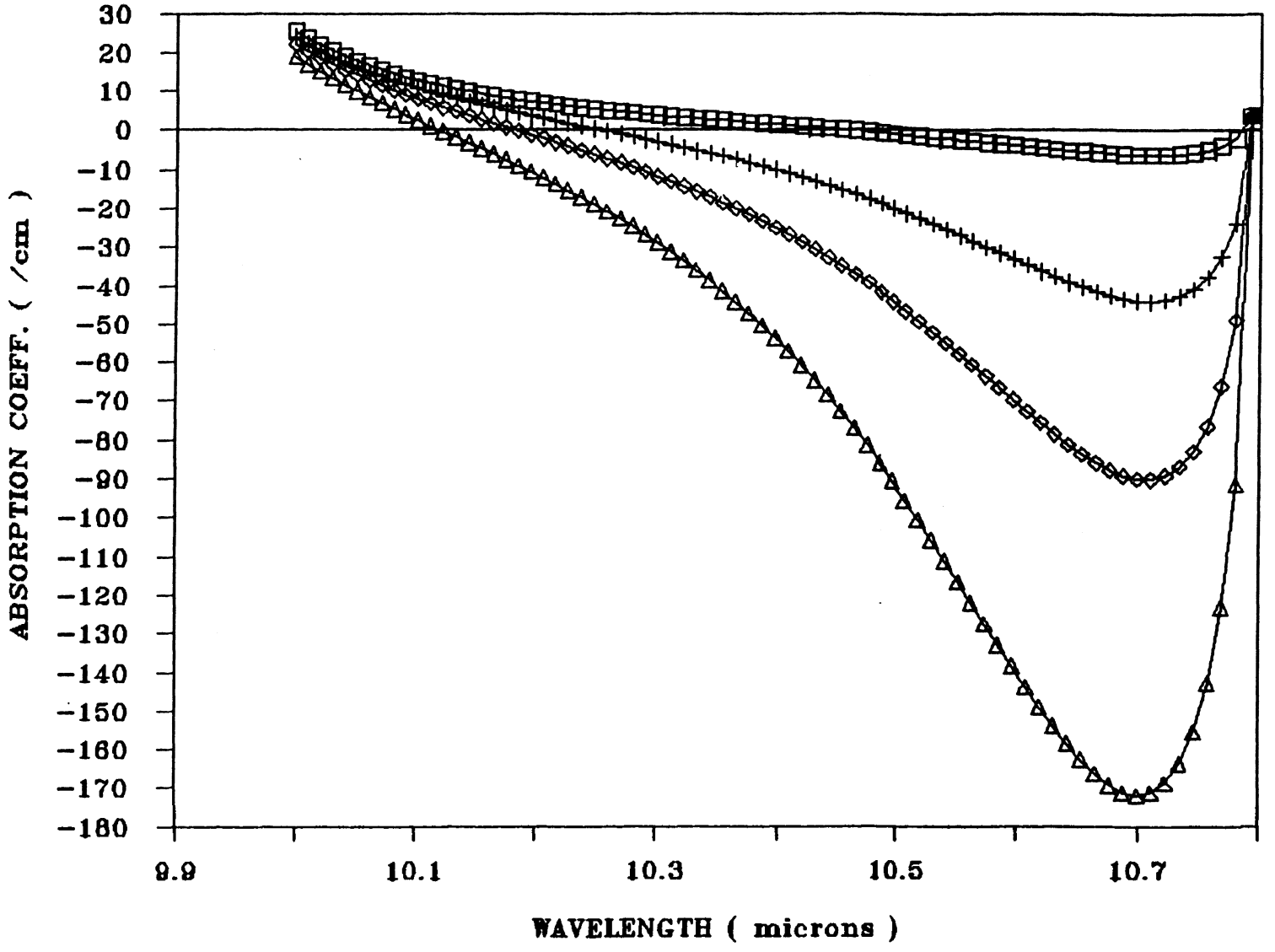
30
20
10
0
-10
-20
-30
-40
-50
-60
-70
-80
-90
-100
-110
-120
-130
-140
-150
-160
-170
-180
ABSORPTION COEFF. (/cm)
9.9
10.1
10.3
10.5
10.7
WAVELENGTH (microns)

Fig.2–6 Model predicted optical gain spectra for 20 % Sn, $Pb_{1-x}Sn_xTe$ with $P = 1 \times 10^{17}$ cm^{-3} at T = 77K (+ I = 1000 W cm^{-2}; <> I = 1250 W cm^{-2}; Δ I = 1500 W cm^{-2})

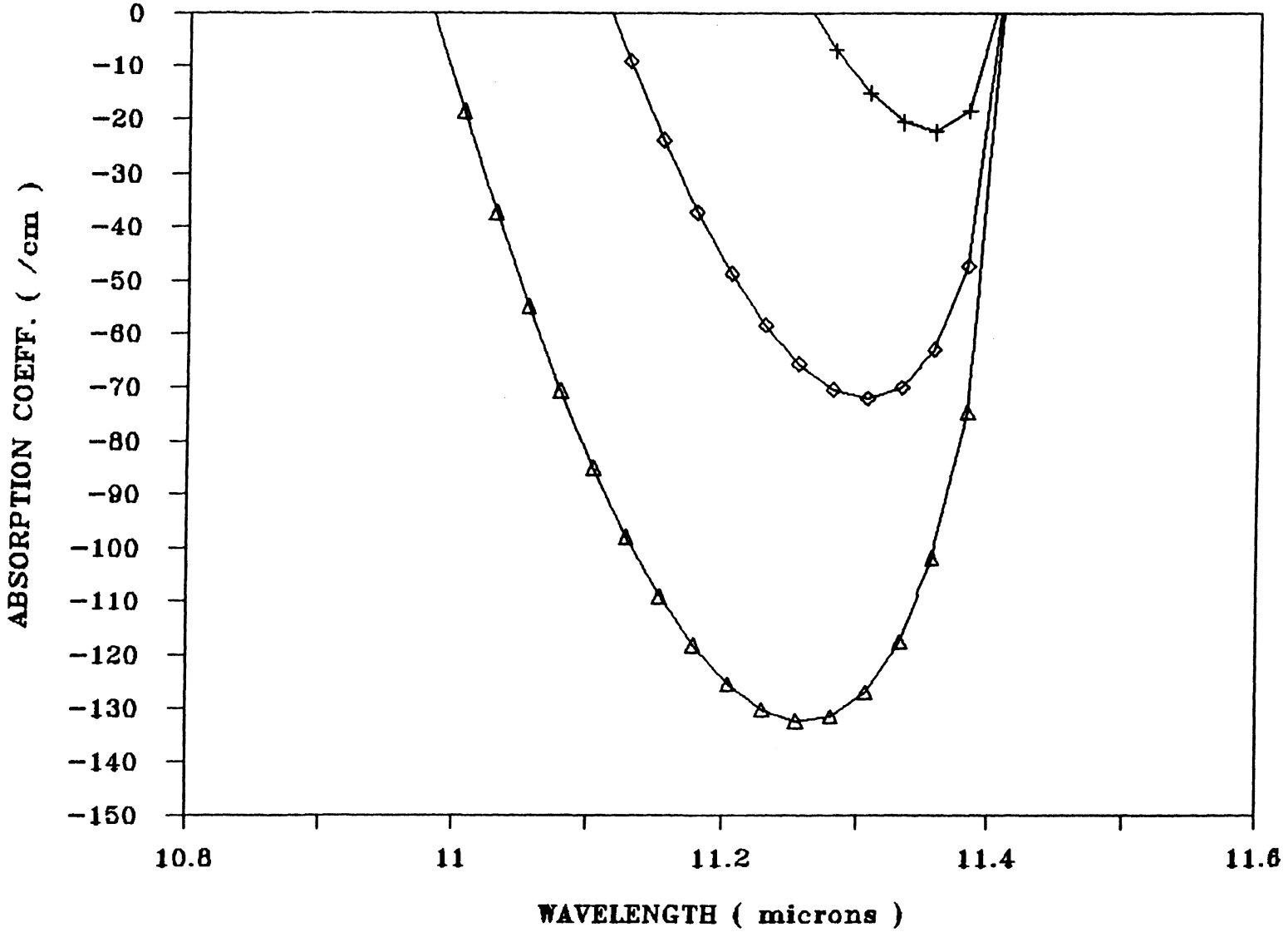
0
-10
-20
-30
-40
-50
-60
-70
-80
-90
-100
-110
-120
-130
-140
-150
ABSORPTION COEFF. (/cm)
10.8
11
11.2
11.4
11.6
WAVELENGTH (microns)

Fig.2–7 Variation of optical transmission with temperature for thermally annealed 18 % Sn, 4 μm thick, $Pb_{1-x}Sn_xTe$ with P = 2 x 10^{17} cm^{-3} at λ = 9.52 μm (□ optical transmission measurements; —— model prediction)

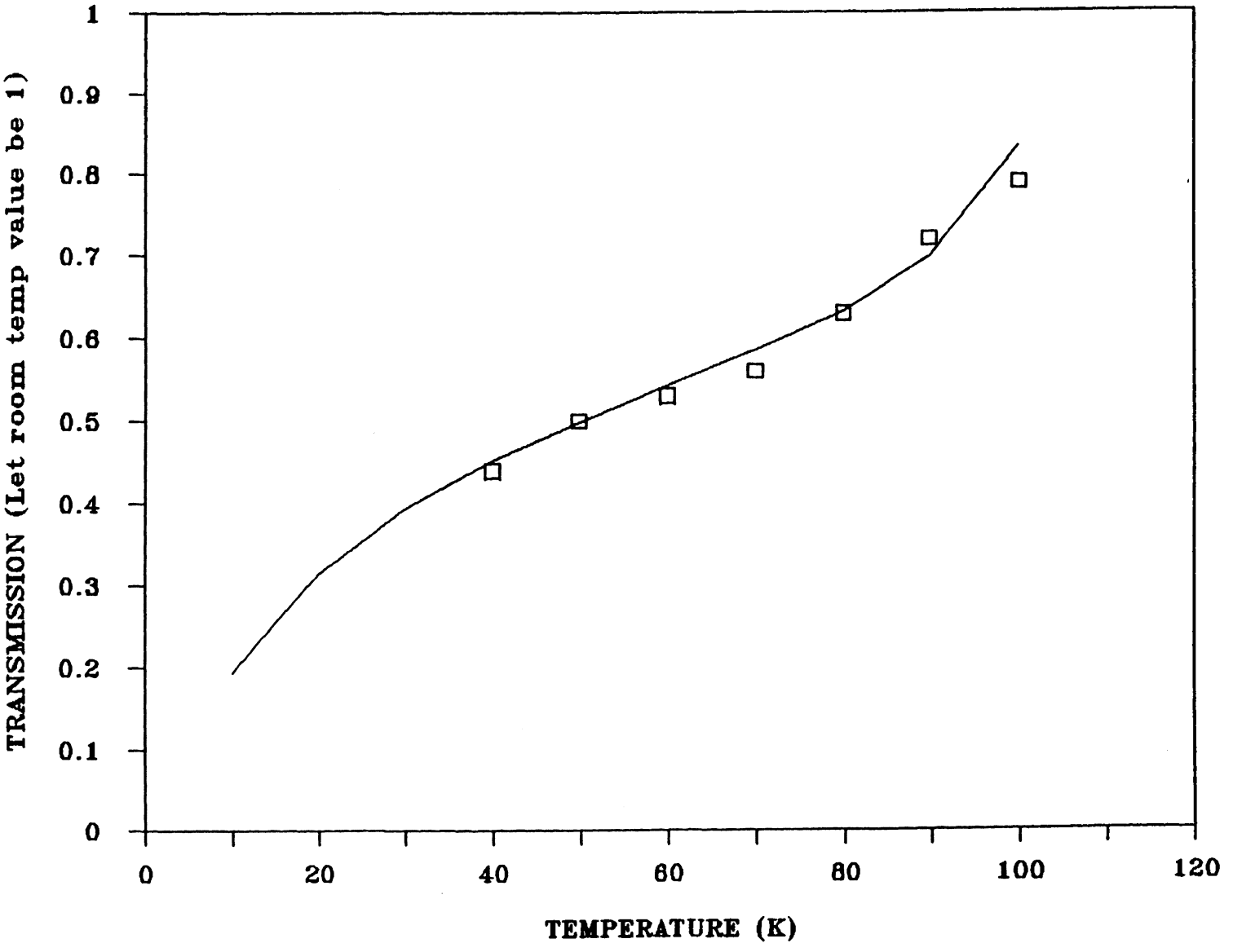
TRANSMISSION (Let room temp value be 1)
1
0.9
0.8
0.7
0.6
0.5
0.4
0.3
0.2
0.1
0
0
20
40
60
80
100
120
TEMPERATURE (K)

2.5 Discussion and Conclusion

It has been shown that an efficient CO_2 laser optically pumped $Pb_{1-x}Sn_xTe$ laser with very low pump intensity should be readily attainable provided that sufficiently low doping density epilayers ($< 10^{17}$ cm^{-3}) can be produced. The model predicted that gain of 200 cm^{-1} can be generated with pump intensity less than 2000 watts cm^{-2} at temperatures below 77K with a quantum efficiency of 10 %, which was obtained from the N_2 laser pumping experiments. However, for room temperature operation, a pump intensity of over 5×10^4 W cm^{-2} with a quantum efficiency of 100 % is needed to create a population inversion in order to produce optical gain in this material. This large increase of the required pump intensity at room temperature is mainly due to the spreading of the free carriers inside the energy bands, which results in much wider gain bandwidth. Hence, much higher free carrier excitation rate is needed so that the required optical gain ($\simeq$ 100 cm^{-1}) at a particular wavelength can be achieved. As far as the availability of a sufficiently powerful pump source is concerned, a CO_2 laser is capable of producing pump intensity well over 10^6 W cm^{-2}. However, with such high pump intensity, the epilayer crystal is subjected to the heating effect. It was estimated that the rate of dissipation of heat in a diode laser is about 10^7 W cm^{-3}. For the CO_2 laser optically pumped $Pb_{1-x}Sn_xTe$ laser at room temperature, the heat dissipation rate is calculated to be 10^7 W cm^{-3}, provided that near quantum limit operation can be accomplished. The required optical gain can be further reduced by using an external cavity with high reflectivity mirrors to minimize the end mirror loss. Therefore, optically pumped $Pb_{1-x}Sn_xTe$ laser with thermal dissipation rate commensurate to that of a diode laser is achievable at room

temperature.

The Hall effect and optical transmission measurements also verified that the high doping density of the epilayers is in fact the cause of the optical absorption edge shifting effect as predicted by the model. It appears that it is possible to use thermal annealing and compensating dopant diffusion methods to obtain epilayers of low enough doping densities to produce CO_2 pumped lasers in Pb salt epilayers by carefully controlling the annealing temperature and time. Nevertheless, the thermal annealing procedures involve exposing the as grown epilayers to atmospheric pressure, which can very easily introduce impurities in the layers, which may degrade the crystal quality of the layers. An alternative is to introduce dopants during the epitaxial growth to compensate the excess p–type tellurium dopants. More efforts are still needed in order to reduce the doping densities of the epilayers to the required doping level for efficient CO_2 laser optical pumping.

CHAPTER 3

MODE–GAIN AND AMPLIFIED SPONTANEOUS EMISSION

3.1 Introduction

It was shown in chapter two that the constraint of the film doping density being less than 1 x 10 ^{17}cm^{-3} for CO_2 laser optically pumped $Pb_{1-x}Sn_xTe$ laser was due to the strong Moss–Burstein shift of the optical absorption edge. This reduction of the optical absorption due to high doping density, however, is only significant at pump wavelengths that are close to the energy band gap wavelengths. If a pump wavelength that is much shorter than the band gap wavelength is chosen, the absorption edge shifting effect will not reduce the optical absorption of the pump source significantly. Hence, by choosing a shorter wavelength laser as pump source, the requirement of low doping density films is eliminated. Important optical properties, such as optical gain and stimulated emission spectrum, can then be measured and compared with the model predictions directly. This direct comparison not only can confirm the accuracy of the model but also further predict whether a CO_2 laser optically pumped $Pb_{1-x}Sn_xTe$ laser is feasible.

In order to ensure that sufficient pump power will be absorbed by the $Pb_{1-x}Sn_xTe$ film, a laser with adequate pump power and short enough wavelength is needed. A N_2 pulsed laser was chosen as the pump source since it has very high pump power, and emits at a short enough wavelength, 0.337 μm, at which the Pb salt materials have very high optical absorption. The N_2 laser also has very short

pulse duration of 300 picoseconds, which is much shorter than the radiative lifetime of the carriers of a few nanoseconds [19] in $Pb_{1-x}Sn_xTe$ and hence the effect of the radiative lifetime can be avoided.

3.2 Nitrogen Laser Optical Pumping Model

The need for a modified model for N_2 laser optical pumping arises from the different characteristics of a pulsed N_2 laser and a cw CO_2 laser. The N_2 laser emits at a wavelength of .337 μm with peak power of 200 KW and pulse duration of 300 picoseconds. The optical absorption coefficient at this wavelength is calculated to be 1.57×10^5 cm^{-1}. This calculation of the absorption coefficient at short wavelength is verified by comparing the measured absorption coefficient at .6328 μm, HeNe laser wavelength with the model prediction. The measured value of the absorption coefficient (9.0×10^4 cm^{-1}) at .6328 μm agree with the calculation to within 1 %. At a high optical absorption coefficient of as high as 1.57×10^5 cm^{-1}, the laser light will only penetrate to a depth of about 0.1 μm from the film surface, and hence the rest of the epilayer film remains unpumped by the laser. Therefore, it is no longer true that the entire 2 to 5 μm thick epilayer is pumped uniformly as in the case of using the CO_2 laser as the pump source and modification to the model is necessary to include this spatial dependence of the excitation levels.

Moreover, the steady state condition which adequately represents a continuous wave laser excitation would not necessarily be valid in the pulse laser pumping condition of pump pulses duration as short as that of the N_2 laser. The

pulse duration of the N_2 laser is about 300 picoseconds, which is comparable to the free carrier lifetime of $Pb_{1-x}Sn_xTe$, that is on the order of a few nanoseconds. [6,7,19] Therefore, a time dependent model is needed to calculate the excess free carrier density.

A model that calculates the optical gain as a function of space (distance from the epilayer surface) and time (within the pulse duration) is described in the following section.

3.2.1 Pulsed Laser Pumping Model

In the cw laser pumping condition, the pump intensity is assumed to be independent of time, but it is necessary in this case to include the time dependent factor of the pump intensity of the N_2 laser. The N_2 laser pulse shape was observed with a 50 picoseconds rise time photodetector and a sampling scope, and was found to be very symmetric to the pulse peak and have rapidly decaying tails. Therefore, the instantaneous pump intensity can be accurately represented by a Guassian function, which has the same characteristics as that of the N_2 laser pulse.

$$I(t) = I_0 \exp\left[-\frac{(t-t_0)^2}{2\Delta t^2} \right] \tag{3.1}$$

I(t) is the instantaneous pump intensity (Watts/cm^2). I_0 is the peak intensity (Watts cm^{-2}). t_0 is the time needed to reach the peak intensity (nanoseconds). Δt

is a characteristic time, such that $I = I_0 \exp(-1/2)$ at $t = t_0 + \Delta t$ (nanoseconds)

Since the excitation level varies with respect to the position along the direction perpendicular to the epilayer surface, the carrier generation rate varies across the epilayer. Hence, the generation rate is a function of both time and space.

$$G(x,t) = \frac{I(t)\left[\exp(-\alpha(x-\Delta x)) - \exp(-\alpha x)\right]}{\hbar\omega \quad \Delta x} \tag{3.2}$$

$\hbar\omega$ is the laser photon energy (eV). Δx is a finite distance chosen to evaluate the the spatially dependent generation rate (μm). α is the optical absorption coefficient at the pump wavelength (cm^{-1})

The carrier generation rate is expected to vary rapidly along the x direction due to the high absorption coefficient ($\simeq 10^5$ cm^{-1}) at the pump wavelength ($\lambda = .337$ μm). Hence, the change of the excess free carrier density can be evaluated by calculating the net generation rate.

$$\Delta N(x,t) = \left[G(x,t) - R(x,t) \right] \Delta t \tag{3.3}$$

the carrier recombination rate includes both the radiative recombination and non–radiative recombination. Unfortunately, there are no experimental values of the diffusion coefficients at such high free carrier density ($\simeq 10^{19} cm^{-3}$) for Pb–salt material is available. Therefore, we've chosen the experimental values for Si and

GaAs [22] at carrier density of 10^{19} cm^{-3} to calculate the change of free carrier density due to carrier diffusion. Since the change of carrier density due to diffusion is only about 10^{17} cm^{-3} within the pulse duration of 300 picoseconds, we've neglected the carrier diffusion effect .

$$R(x,t) = R_{non-rad}(x,t) + R_{rad}(x,t) \tag{3.4}$$

In eq.(3.3), the generation rate is no longer equal to the recombination rate. This non steady–state condition arises from the short pulse duration of the N_2 laser, which does not allow the carrier density to have enough time to reach steady–state. The radiative recombination rate is taken to be the spontaneous emission rate

$$R_{rad}(x,t) = R_{spon}(x,t) \tag{3.5}$$

The initial spontaneous emission rate at the beginning of the laser pulse ($t = t_o$), when there is no separation of the quasi–fermi levels (unpumped condition), is known. Hence, the subsequent spontaneous emission rate during the laser pulse can be calculated.

Auger recombinations are non–radiative recombination processes, by which free carriers become bound carriers by colliding with other free carriers and losing energy by causing lattice vibrations. The Auger recombination term has a cubic dependence of the free carrier density (N^3), and becomes dominant for high excess free carrier density. Auger recombination lifetimes as short as hundreds of

picoseconds have been calculated according to Roseman. [19] This lifetime (τ_{n-r}) is given by

$$\frac{1}{\tau_{n-r}} = C\,(P + N)\,\frac{P\,N - P_o N_o}{N - N_o} \tag{3.6}$$

P and N are the instantaneous carrier densities for holes and electrons. P_o and N_o are the carrier densities for hole and electron at equilibrium; C is a parameter given by

$$C = \frac{3\pi^{5/2}}{2}\,\frac{e^4\,P_t^{\,4}}{\hbar}\,\frac{\sqrt{r(kT)}}{E_g^{\,2}} \tag{3.7}$$

where $P_t = 4.74 * 10^{-8}$ eV–cm

$P_l = P_t(10.25 + 6.56x)^{-1/2}$ eV–cm

$r = (P_l/P_t)^2$

eq.(3.3) can now be rewritten as

$$\Delta N(x,t) = \left[G(x,t) - R_{spon}(x,t) - \frac{\Delta N(x, t-\Delta t)}{\tau_{n-r}}\right] \Delta t \tag{3.8}$$

the free electron density is given by

$$N(x,t) = N(x,t-\Delta t) + \Delta N(x,t) \tag{3.9}$$

Following the model described, the free carrier density profile in the film can be calculated for a specific pump intensity. This free carrier density profile can then be used to calculate the spatial distribution of the complex dielectric constant in the film.

3.2.2 Spatial Variation of the Complex Dielectric Constant

In chapter two, we discussed the factors that affect the values of the optical gain and refractive index in $Pb_{1-x}Sn_xTe$ material. It was shown that the presence of optical gain is due to the inverted population, which is represented by the free electron–hole pairs created in the conduction and valence bands of the semiconductor. We also discussed the importance of the free carrier contribution to the refractive index due to the very small effective mass values of the energy bands and the long wavelength at which this material emits. Hence, any change of the free carrier density will cause both the optical gain and refractive index to change accordingly.

As we can see from the previous section, the free carrier density profile in the epilayer changes drastically from the film surface to a depth of about .1 μm from the surface during the laser pulse. This free carrier density spatial profile creates a pumped (gain) and unpumped (loss) regions within the epilayer. In order to compare the measured net gain values with the model predictions, the knowledge of the overlapping integral of the optical field and the gain and loss regions is essential. If the optical field is well confined within the gain region, the measured net gain will be directly comparable with the predicted optical gain in the gain region. If the optical field is not confined within the gain region, the predicted net gain will be determined by the overlapping integral of the optical field and the gain and loss regions. Since the size of the optical field is controlled by the complex dielectric constant profiles within the epilayer, it is necessary to determine the complex dielectric constant profile so that the size of the optical field can be

evaluated.

The relations between the complex dielectric constant, and the index of refraction and optical gain are very well known (Appendix A). The dielectric constant can be written in two parts, the real and imaginary parts of the dielectric constant.

$$\epsilon_c = \epsilon_r + i\epsilon_i \tag{3.10}$$

where ϵ_c is the complex dielectric constant, ϵ_r is the real part of the dielectric constant, and ϵ_i is the imaginary part of the dielectric constant. The index of refraction can also be written in a similar way

$$n_c = n_r + in_i \tag{3.11}$$

the dielectric constant can be written in terms of the real and imaginary parts of the index of refraction

$$\epsilon_r = n_r^2 - n_i^2 \tag{3.12}$$

$$\epsilon_i = 2\, n_r n_i \tag{3.13}$$

n_r is the real part of the index of refraction, which is usually referred to as the refractive index, and n_i is the imaginary part of the index of refraction, which can be written in terms of the optical absorption (gain) coefficient (Appendix A).

$$n_i = \frac{\alpha \, c}{2 \, \omega} \tag{3.14}$$

Fig.3–1 and 3–2 show the spatial variation of the real and imaginary parts of the dielectric constant at a pump intensity of 20 MW cm^{-2}. In fig.3–1, the real part of the dielectric constant increases with distance from the surface. This change of the real part of the dielectric constant is contributed by the free carrier effect described in chapter two. Fig.3–1 also shows that the refractive index decreases as the free carrier density increases towards the film surface and the index step increases with longer wavelength. An optical waveguide is a structure of material in which the optical field is well confined within the desired region in the structure. It requires that the refractive index be higher in the confining region than the region surrounding it. However, the real dielectric constant profile shown in fig.3–1 has a lower refractive index value in the gain region. This index step forces the waveguide modes to be out of the gain region, which is close to the epilayer surface, and into the loss region, which is away from the epilayer surface. In fig.3–2, the imaginary part of the dielectric constant varies from large positive to large negative values as the distance from the surface increases. The long wavelength emission sees moderate optical gain in the pumped region and very small optical loss in the unpumped region. The short wavelength emission sees very high optical gain in the pumped region as well as very high optical loss in the unpumped region. These profiles reveal that the physical size of the waveguide modes will depend on the emission wavelength. Therefore, a complex waveguide model is needed to evaluate the mode size at various wavelengths, so that the mode–gain and A.S.E.

Fig.3–1 Model predicted real part of the dielectric constant for 16 % Sn, $Pb_{1-x}Sn_xTe$ with P = 5 x 10^{17} cm^{-3} at T = 77K at a peak pulse intensity of 20 MW cm^{-2} (□ $\lambda = 9.5\mu m$; + $\lambda = 8.5\ \mu m$; <> $\lambda = 7.5\ \mu m$; Δ $\lambda = 6.5\ \mu m$)

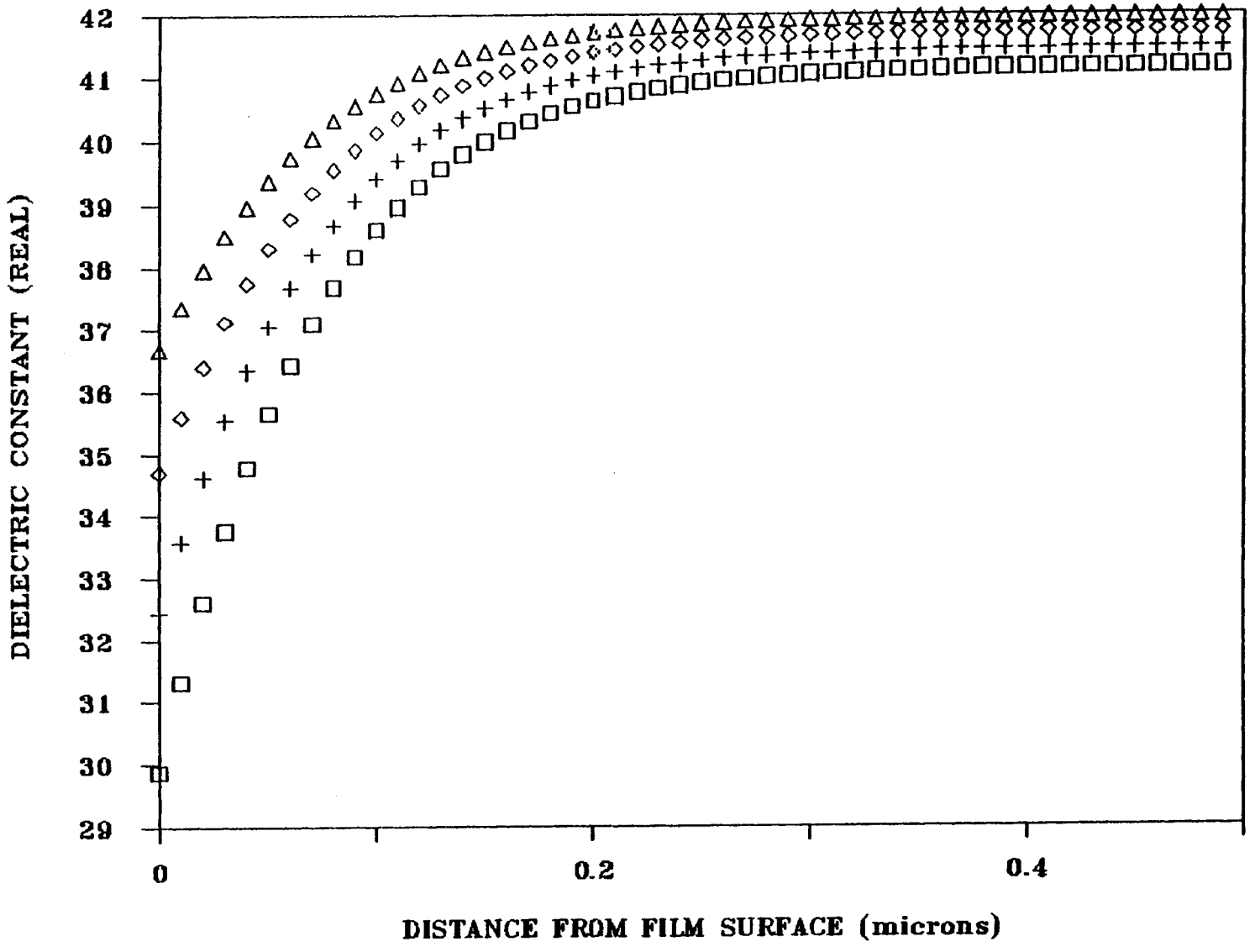
42
41
40
39
38
37
36
35
34
33
32
31
30
29
DIELECTRIC CONSTANT (REAL)
0
0.2
0.4
DISTANCE FROM FILM SURFACE (microns)

Fig.3–2 Model predicted imaginary part of the dielectric constant for 16 % Sn, $Pb_{1-x}Sn_xTe$ with P = 2 x 10^{17} cm^{-3} at T = 77K at a pump intensity of 20 MW cm^{-2} (□ λ = 9.5 μm; + λ = 8.5 μm; <> λ = 7.5 μm; Δ λ = 6.5 μm)

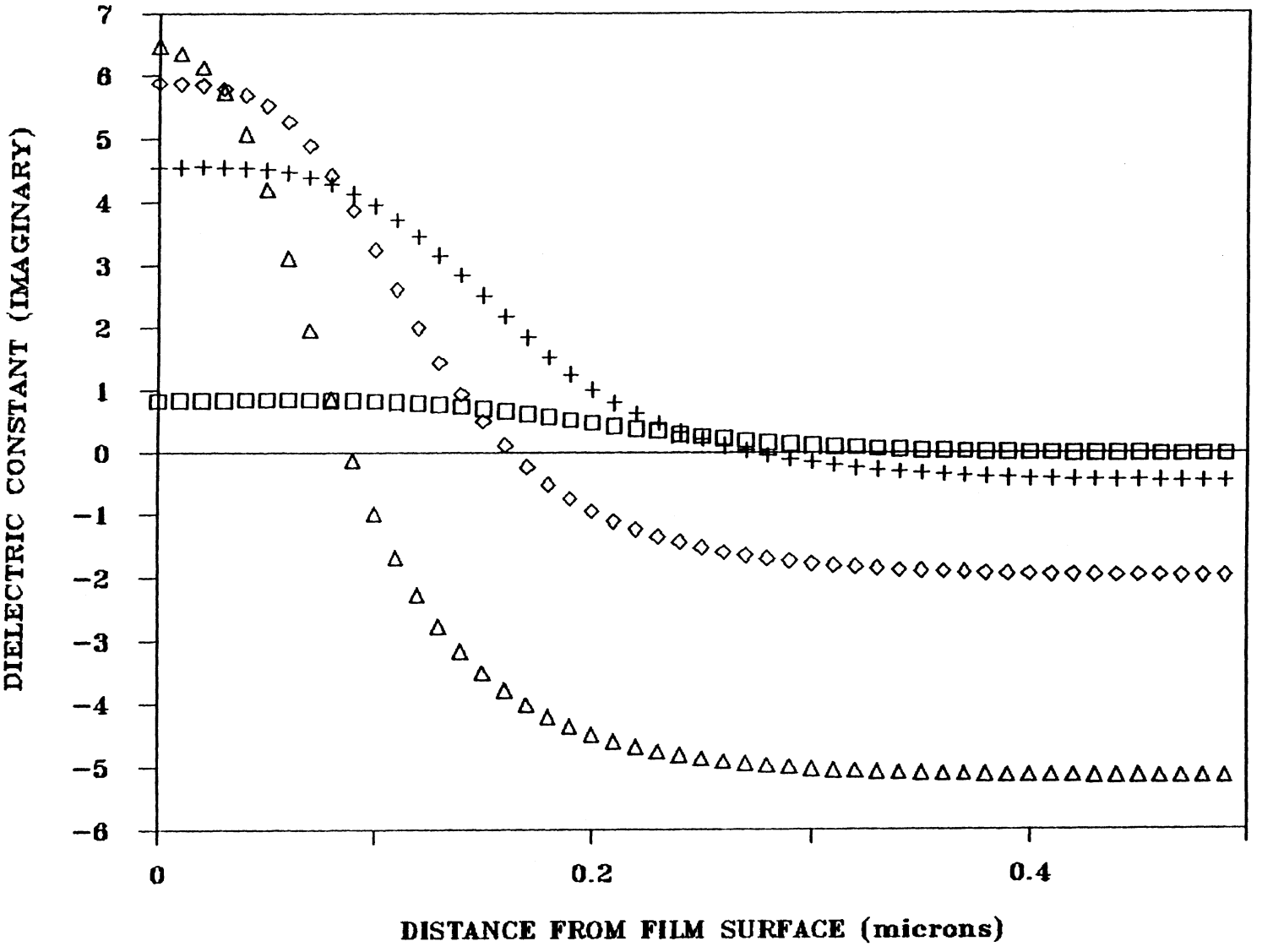
DIELECTRIC CONSTANT (IMAGINARY)
7
6
5
4
3
2
1
0
−1
−2
−3
−4
−5
−6
0
0.2
0.4
DISTANCE FROM FILM SURFACE (microns)

spectra can be predicted and compared with the experimental results.

3.2.3 Transverse Waveguide Modes

In order to solve the wave equation with a dielectric constant profile predicted in section 3.2.3, we have to use a numerical method to seek solutions. However, the exact shape of the optical field is not as important for our purpose as the optical mode size. Therefore, a complex step index model, which approximates the complex dielectric constant profiles to step like profiles, was chosen to estimate the mode–size of the waveguide mode for simplicity. There are three possible results from the model. Firstly, the optical field is confined in the gain region, and the net gain will be the same as the optical gain in the gain region. Secondly, the optical field is overlapping both the gain and loss regions, and the net gain can be evaluated by integrating the product of the optical field and the optical gain and loss profile over the entire epilayer. Thirdly, there is no stable optical field exist for the complex dielectric profiles. Since there is a very large index step ($\Delta N \simeq 4$) between the $Pb_{1-x}Sn_xTe$ and the BaF_2 interface, a well confined optical mode must exist within the epilayer according to a simple slab waveguide calculation. Therefore, in the case of no solution to the model, the net gain can still be evaluated by integrating the gain and loss over the entire epilayer.

The solution of the optical modes are determined by the Maxwell's equations (Appendix B).

$$\frac{\partial^2 A}{\partial x^2} = \beta^2 A - \frac{\omega_0^2 \epsilon}{c^2} A \tag{3.15}$$

A is the magnitude of the transverse electric field. ω_0 is the frequency of the electric field. ϵ is the complex dielectric constant. β is the propagation constant. c is the velocity of light in vacuum

For a wave propagating in the z direction, we seek a solution of the general form

$$E(x,t) = A(x,t) \sin(\frac{\pi m z}{l}) \exp(i\omega_0 t) \tag{3.16}$$

where m is an integer. The sine term forces the field to be zero at the semiconductor –air interface so that a standing wave pattern can be established inside the optical cavity. For simplicity, a step complex dielectric constant model was chosen to estimate the mode size. The dielectric constant is taken to be of the form

$$\epsilon(x) = \epsilon_0' + \delta\epsilon_0'' + i\epsilon_g'' \qquad \text{in } (0,d) \tag{3.17}$$

$$\epsilon(x) = \epsilon_0' \qquad - i\epsilon_1'' \qquad \text{in } (d,\infty) \tag{3.18}$$

ϵ_0' is the basic contribution to index. $\delta\epsilon_0''$ is the step change of the dielectric constant due to the presence of excess free carriers and is negative in this case. $\epsilon_g''(\epsilon_1'')$ describes the negative (positive) absorption of the A.S.E. in the pumped

Fig.3–3 Model predicted Mode–Gain spectra for 18 % Sn, $Pb_{1-x}Sn_xTe$ with $P = 5 \times 10^{17}$ cm^{-3} at T = 77K at a pump intensity of 20 MW cm^{-2} (□ th = 2.0 μm; + th = 1.0 μm; <> th = 0.5 μm)

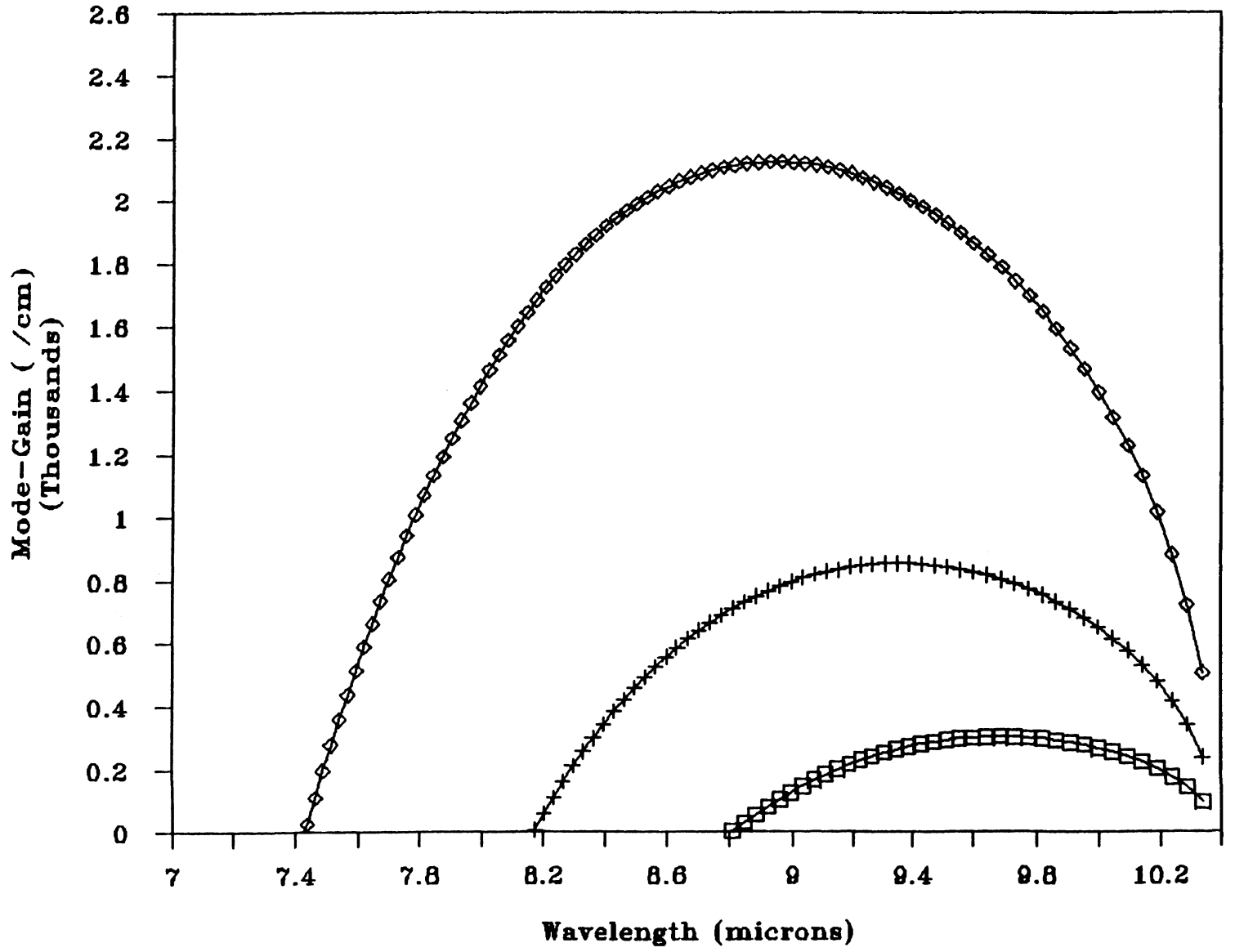
Mode-Gain (/cm)
(Thousands)
2.6
2.4
2.2
2
1.8
1.6
1.4
1.2
1
0.8
0.6
0.4
0.2
0
7
7.4
7.8
8.2
8.6
9
9.4
9.8
10.2
Wavelength (microns)

Fig.3–4 Model predicted A.S.E. spectra for 18 % Sn, $Pb_{1-x}Sn_xTe$ with P = 5 x 10^{17} cm^{-3} at T = 77K at a pump intensity of 20 MW cm^{-2} (□ th = 2.0 μm; + th = 1.0 μm; <> th = 0.5 μm)

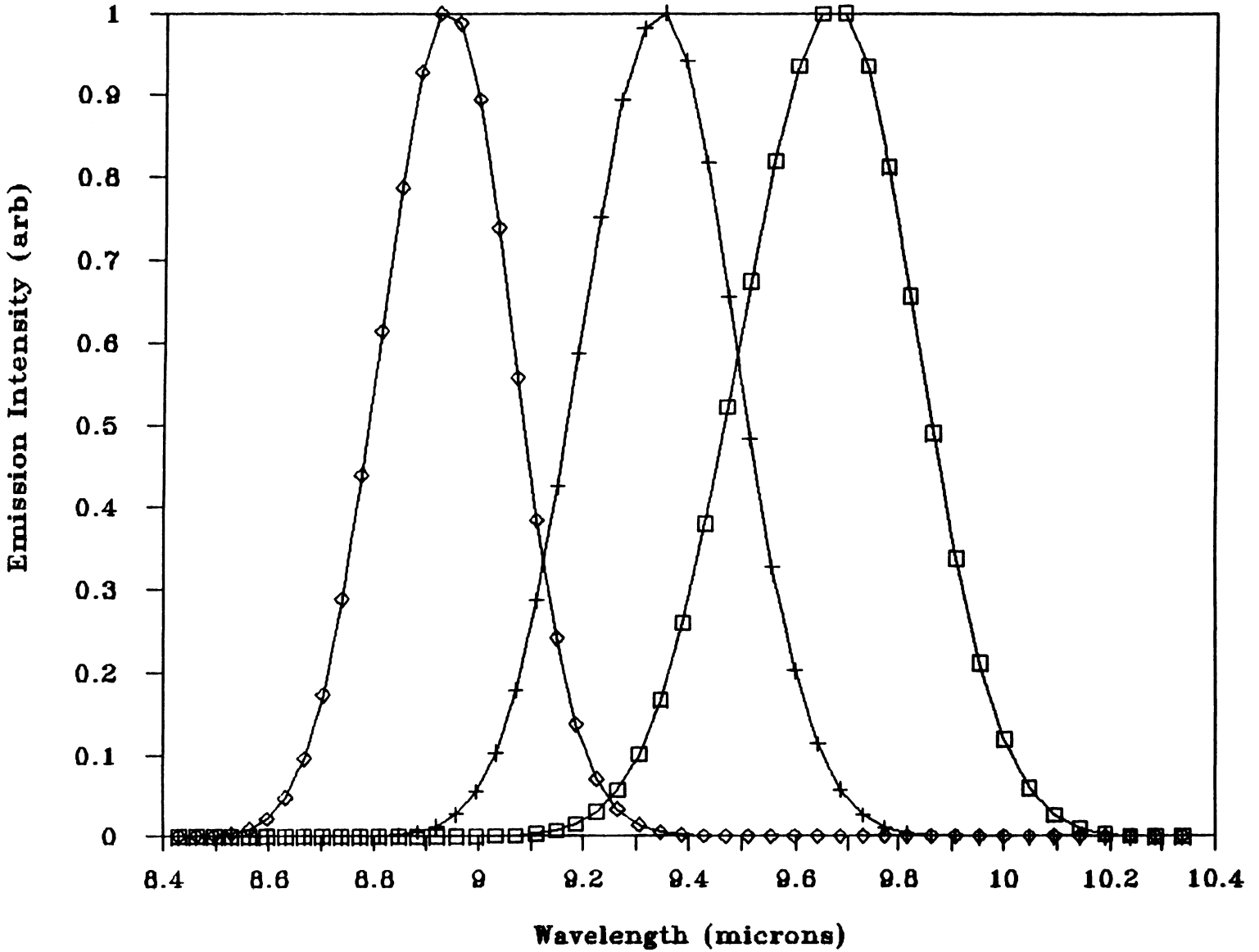
Emission Intensity (arb)
1
0.9
0.8
0.7
0.6
0.5
0.4
0.3
0.2
0.1
0
8.4
8.6
8.8
9
9.2
9.4
9.6
9.8
10
10.2
10.4
Wavelength (microns)

Fig.3–5 Model predicted Mode–Gain spectra for 18 % Sn, $Pb_{1-x}Sn_xTe$ with th = 2 μm at T = 77K at a pump intensity of 20 MW cm^{-2} (□ P = 3 x 10^{17} cm^{-3}; + P = 5 x 10^{17} cm^{-3}; <>, P = 1 x 10^{18} cm^{-3})

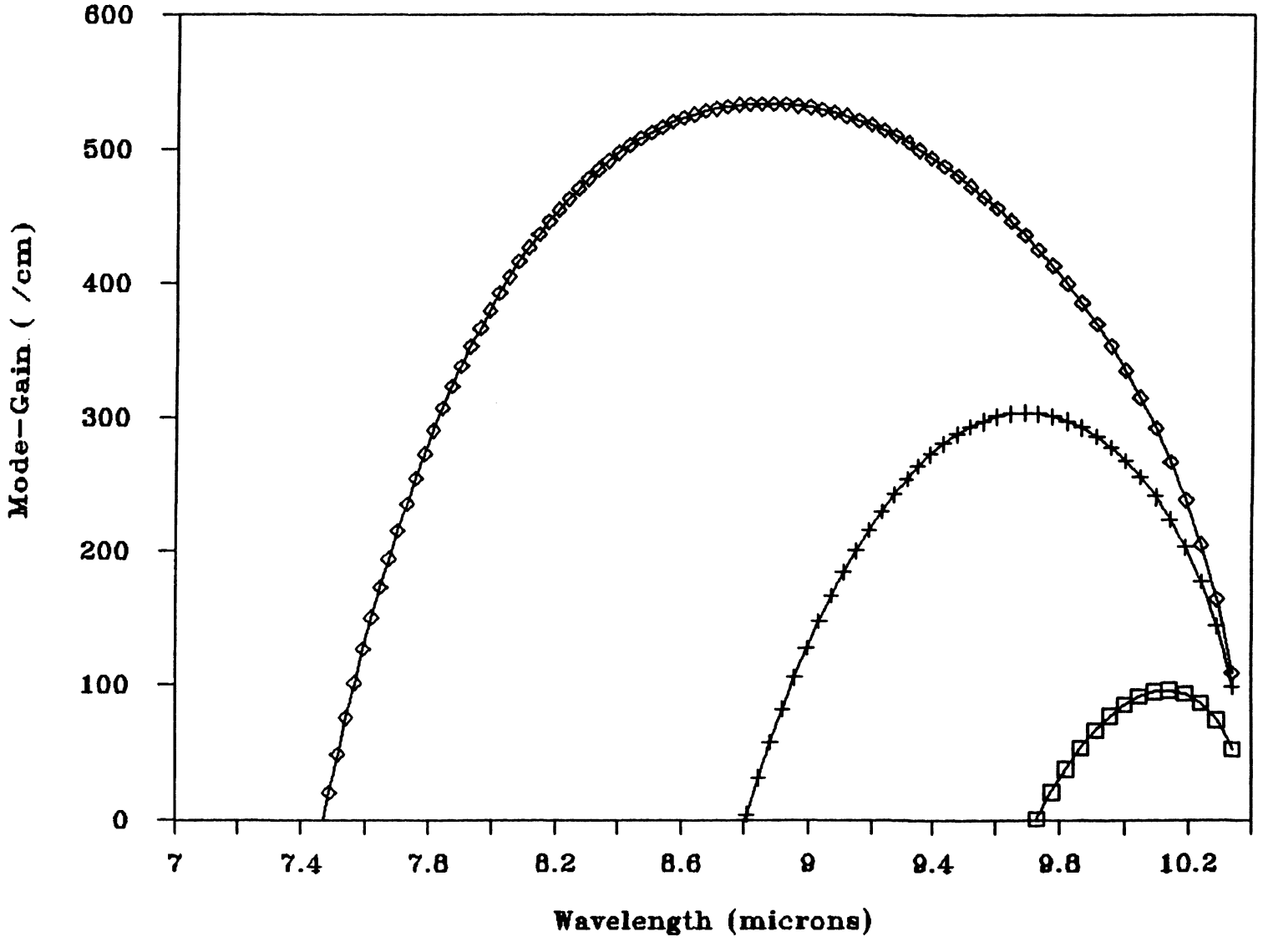
600
500
400
300
200
100
0
Mode-Gain (/cm)
7
7.4
7.8
8.2
8.6
9
9.4
9.8
10.2
Wavelength (microns)

Fig.3–6 Model predicted A.S.E. spectra for 18 % Sn, $Pb_{1-x}Sn_xTe$ with th = 2 μm at T = 77K at a pump intensity of 20 MW cm^{-2} (□ P = 3 x 10^{17} cm^{-3}; +, P = 5 x 10^{17} cm^{-3}; <>, P = 1 x 10^{18} cm^{-3})

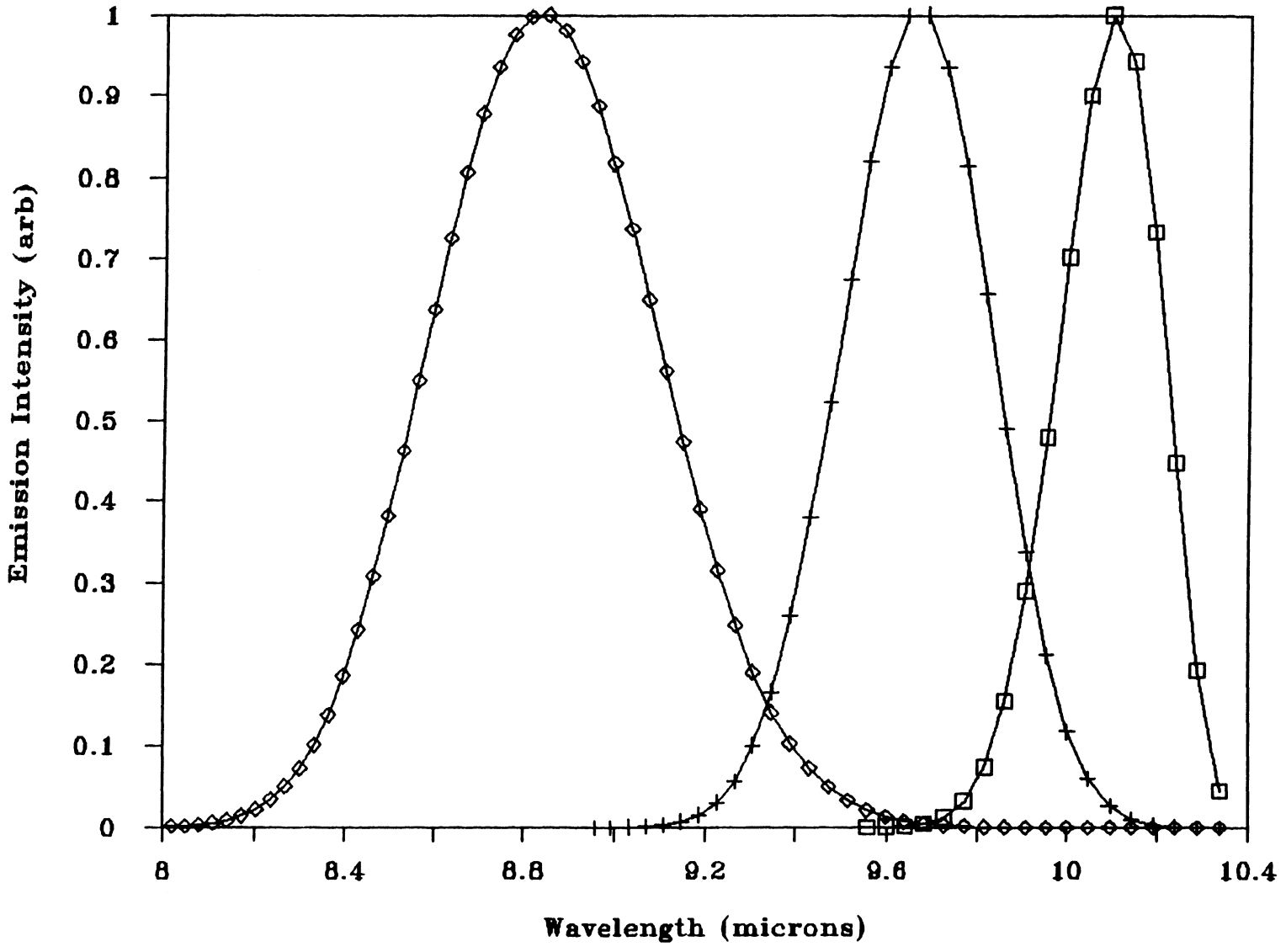
Emission Intensity (arb)
1
0.9
0.8
0.7
0.6
0.5
0.4
0.3
0.2
0.1
0
8
8.4
8.8
9.2
9.6
10
10.4
Wavelength (microns)

effects of the A.S.E. spectra for different doping density epilayers. Again, the emission peak is shifted from 10.1 μm to 8.9 μm for a change of epilayer doping density from 3×10^{17} cm^{-3} to 1×10^{18} cm^{-3}. However, the emission bandwidth in this case is very sensitive to the change of the doping density. The emission width changes from approximately 0.2 μm to 0.6 μm as the doping density changes from 3×10^{17} cm^{-3} to 1×10^{18} cm^{-3}.

In summary, the model predicts the shifting of the emission peak to longer wavelength for thicker epilayer and lower doping density, and the narrowing of the emission bandwidth for lower doping density.

3.3 Experimental Results and Comparisons

Mode–gain was measured for various epilayer thicknesses by using the stripe pumping method described in chapter one. The emission spectra for various samples were also measured so that they can be compared with the predicted spectra. From the spectral width and peak, we can verify the effect of spectral narrowing and wavelength tuning due to the overlap of the optical field and the loss region as predicted by the model presented in the previous section.

3.3.1 Experimental Set–Up

Before going into all the experimental results, this section will describe the set–ups used in the experiments.

Fig.3–7 shows the experimental set–up for the optical gain measurements. A PRA LN–103 pulsed Nitrogen laser was used as the pump source. The laser gives output energy of about 60 μJ per pulse with a pulse duration of about 300 picoseconds at .337μm wavelength. A visible HeNe laser (emits at .6328 μm, red) was lined up with the N_2 laser as a beam finder. The laser light was focused to a stripe about 1 cm long and 100 μm wide by a combination of a short focal length cylindrical lens and a long focal length spherical lens. The A.S.E. emission passed through a KRS–5 window, which is an excellent transmitter from .6μm to beyond 20 μm wavelengths, and was collected by a f/1 1–inch diameter Ge focusing lens and imaged onto a liquid nitrogen cooled HgCdTe detector. The detected signal was connected to a Lecroy 9400 digital oscilloscope, which is capable

Fig.3–7 Schematic for the experimental set–up used for optical gain measurements

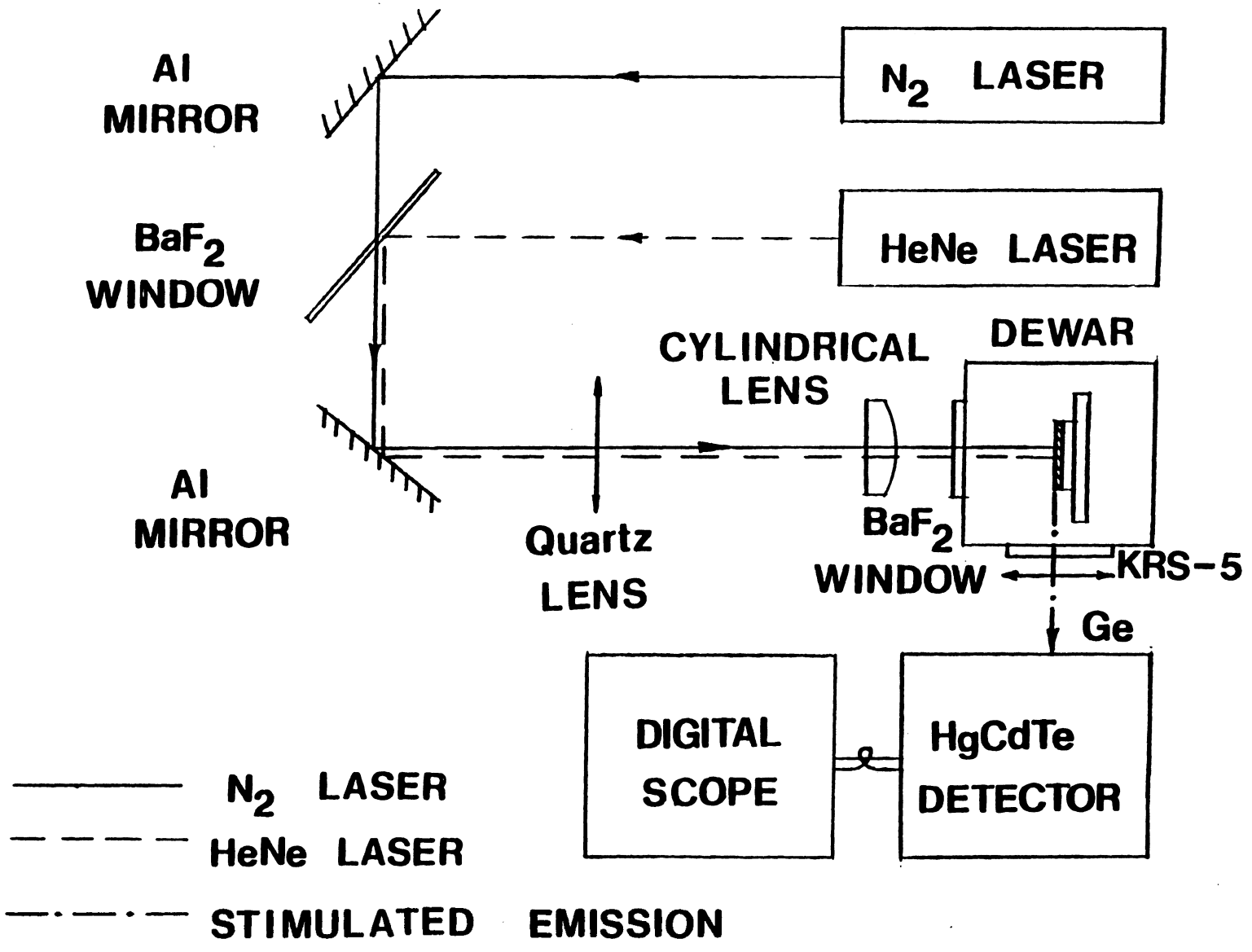
Al
MIRROR
N_2 LASER
BaF_2
WINDOW
HeNe LASER
CYLINDRICAL
LENS
DEWAR
Al
MIRROR
Quartz
LENS
BaF_2
WINDOW
KRS-5
Ge
DIGITAL
SCOPE
HgCdTe
DETECTOR
N_2 LASER
HeNe LASER
STIMULATED EMISSION

of performing real time signal averaging. This signal average improves the signal to noise ratio of the detected signal. The digital scope was triggered by the detected N_2 laser pulse. The laser stripe length l, was varied by moving the position of a sharp razor blade across the laser stripe. The razor blade was mounted on a very accurate micropositioner. A variable neutral density filter was also used to attenuate the laser intensity so that mode–gain numbers for various pump intensities can also be measured.

A similar set–up to that of fig.3–7 was used for the A.S.E. spectrum measurements with the exception that the emission intensity was collected by a f/1 2–inch diameter focusing lens and imaged onto the entrance slit of a Jarrell–Ash 1/4–meter monochromator. The 1/4–meter monochromator has a 10 μm blazed diffraction grating and a resolution of 0.01 μm (100 Å). The output of the monochromator was imaged directly onto the detector.

Both the KRS–5 and Ge material have very high optical absorption at N_2 laser wavelength (.337 μm). Therefore, both the KRS–5 window and the Ge lens act naturally as absorption filters, which cut off all the scattered N_2 laser light.

The samples were glued with silver print on the heat sink in the Liquid Helium dewar, which is capable of operating at close to liquid Helium temperature, 4.2K. However, most of our experiments were done at 77K instead, using liquid nitrogen as the coolant.

3.3.2 Experimental Results

Optical gain was measured by recording the emission intensity vs. stripe length, as described in chapter one, for three different samples with different layer thicknesses. The emission spectrum was also measured to compare with the predicted A.S.E. spectrum.

Fig.3–8 is the emission intensity vs. stripe length results for a 2.3μm thick, 18% Sn, $Pb_{1-x}Sn_xTe$ layer grown on BaF_2 substrate. Optical net gain values of 370 cm^{-1} , 300 cm^{-1}, and 110 cm^{-1} with 10 % uncertainties were measured for pump intensities of 20 MW cm^{-2}, 6.4 MW cm^{-2} and 3.6 MW cm^{-2} respectively. The linear part of the intensity vs. strip length curve in the logarithm scale shows that the emission intensity varies exponentially with the pump stripe length. This exponential dependence also shows optical gain is present. The change of the measured gain numbers with respect to the pump intensity verifies that this is a genuine optical gain effect due to optical excitation according to eq.(1.2). Fig.3–9 shows the corresponding curve for a different sample with a 4 μm thick, 18% Sn, $Pb_{1-x}Sn_xTe$ layer on BaF_2 substrate. The optical net gain value was measured to be 220 $\pm$ 20 cm^{-1} for a pump intensity of 20 MW cm^{-2}. The change of the gain generated in the two samples by the same pump intensity is clearly related to the epilayer thicknesses as predicted in section 3.2.4. The below threshold gain region was also observed in the region close to the left bottom corner in fig.3–9. Optical net gain value of 100 cm^{-1} was also measured for a multilayer sample at a pump intensity of 20 MW cm^{-2}. This measured net gain is consistent with the model prediction.

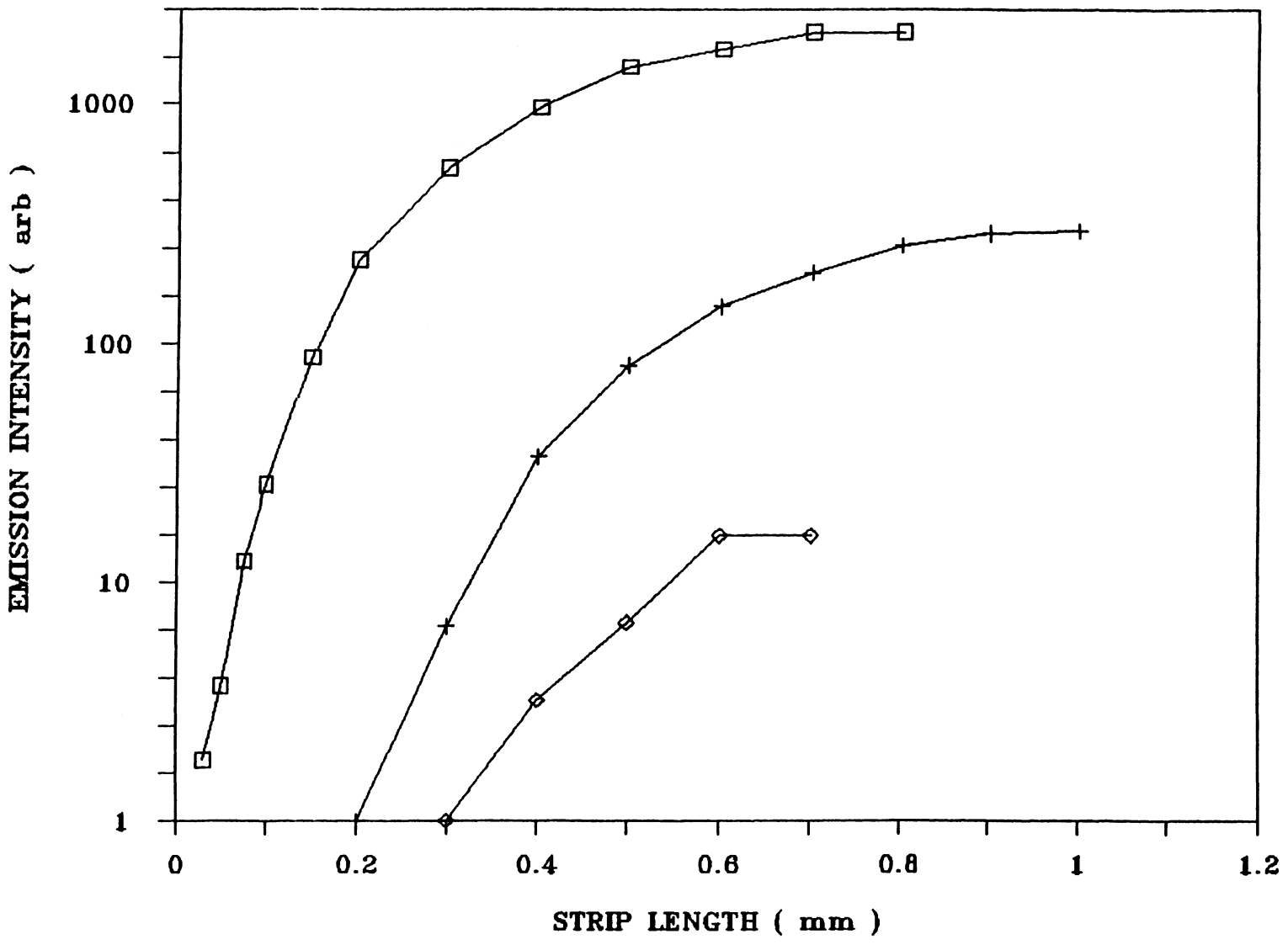
EMISSION INTENSITY (arb)
1000
100
10
1
0
0.2
0.4
0.6
0.8
1
1.2
STRIP LENGTH (mm)

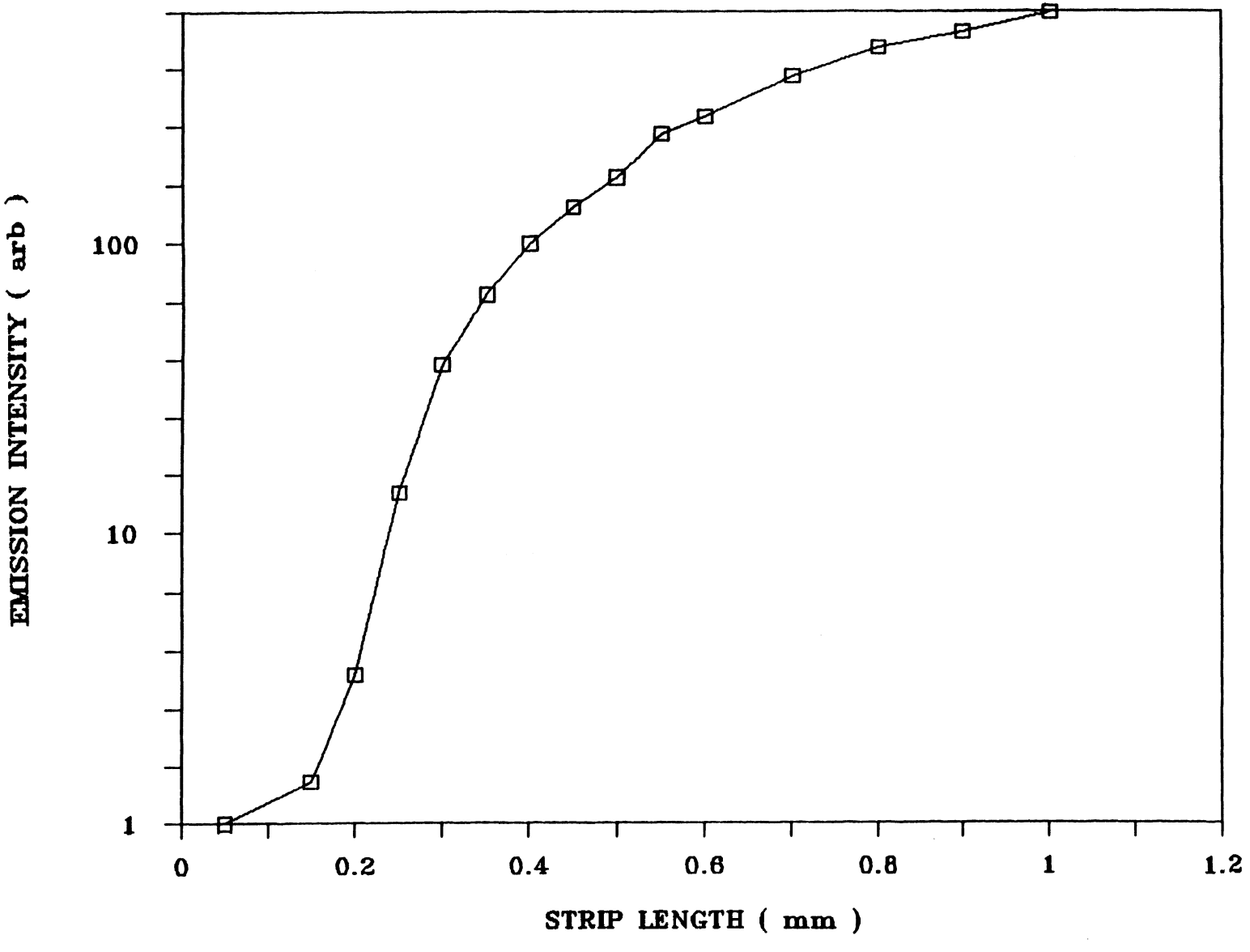
EMISSION INTENSITY (arb)
100
10
1
0
0.2
0.4
0.6
0.8
1
1.2
STRIP LENGTH (mm)

So far we've only reported the net gain measurement (the mode–gain integrated over the entire mode–gain spectrum); the mode–gain spectral shape and width are, nevertheless very important in determining the laser characteristics. In order to measure the net gain spectrum, the emission intensity is cut down by a factor of about 100 due to the power loss from passing the emission signal through the monochromator, and measuring the emission intensity at below gain saturation points. This power attenuation makes it impossible to measure the net gain spectrum.

Fortunately, the emission spectrum measurement requires a lower light intensity. Therefore, in stead of measuring the net gain spectrum, we measured the emission spectrum. Fig.3–10 shows the emission spectrum of the 2.3 μm thick, 18% Sn layer. The emission intensity peaks at 9.42 μm with a spectral width of about .42 μm at a pump intensity of 20 MWatts.cm^{-2}. The spectral shape is asymmetric, and has a sharper falling edge on the long wavelength side.

According to the model, the thicker the epilayer is, the less net gain is present for a homogeneous layer. Hence, by increasing the thickness of the film, the net gain should be reduced to very small number and the spectral width of the emission should be about 3 to 4 μm which is much broader than the amplified spontaneous emission spectral width of .42 μm that was measured for the 2.3 μm thick sample. Hence, the spectral width can be used as a differentiation between spontaneous and stimulated emission. In an attempt to obtain the broad spectral width of the spontaneous emission, a 20 μm thick, 20% Sn, $Pb_{1-x}Sn_xTe$ epilayer was grown on BaF_2 and the emission spectrum of that sample was also obtained. The net gain is expected to be negative (net loss) for a 20 μm thick uniform film and

the emission spectral width is expected to be about 3.5 μm. Fig.3–11 shows the emission peak at 10.98 μm with a spectral width of about .18 μm, which is even narrower than the .42 μm spectral width of the 2.3 μm thick sample. This very narrow emission spectral width indicates that optical net gain was present and the spectrum has the characteristics of stimulated emission. In order to verify that this is not emission from the surface impurity states but that it is indeed stimulated emission from $Pb_{1-x}Sn_xTe$ crystal, the same sample was etched in chemical etchant and about 2 μm of the surface layer was etched off. The emission spectrum of the etched sample was measured and displayed in fig.3–12. The emission intensity again peaks at about 10.98 μm but with a slightly broader spectral width of about .26 μm. The narrow spectral width observed after chemical etching suggest that the observed spectral width was not due to surface effect but was genuine emission from the Pb salt crystal.

These results are consistent with the model's predictions when the inhomogeneity of the doping density in the epilayer is taken into account. It was found by Y. Yang et al [21] that the Sn atoms have the tendency to diffuse out of the epilayer to make it Tellurium rich. Hence, the surface doping density tends to be lower than the doping density inside the epilayer due to the presence of excess Tellurium atoms in the epilayer. It was also reported that doping density gradient typically of 4×10^{16} cm^{-3} μm^{-1} was present in the epilayer. Since the refractive index of $Pb_{1-x}Sn_xTe$ depends strongly on the free carrier density, refractive index step of about 0.1 is present in the first 1 μm from the film surface. It's been calculated from a simple slab waveguide model that index step of 0.1 with a confining thickness of 1 μm is sufficient to confine the optical field in that 1 μm

Fig.3–10 Emission spectrum for the 2.3 μm thick, 18% Sn epilayer with P = 6 x 10^{17} cm^{-3} at T = 77K at I = 20 MW cm^{-2} (—— model prediction; + experimental)

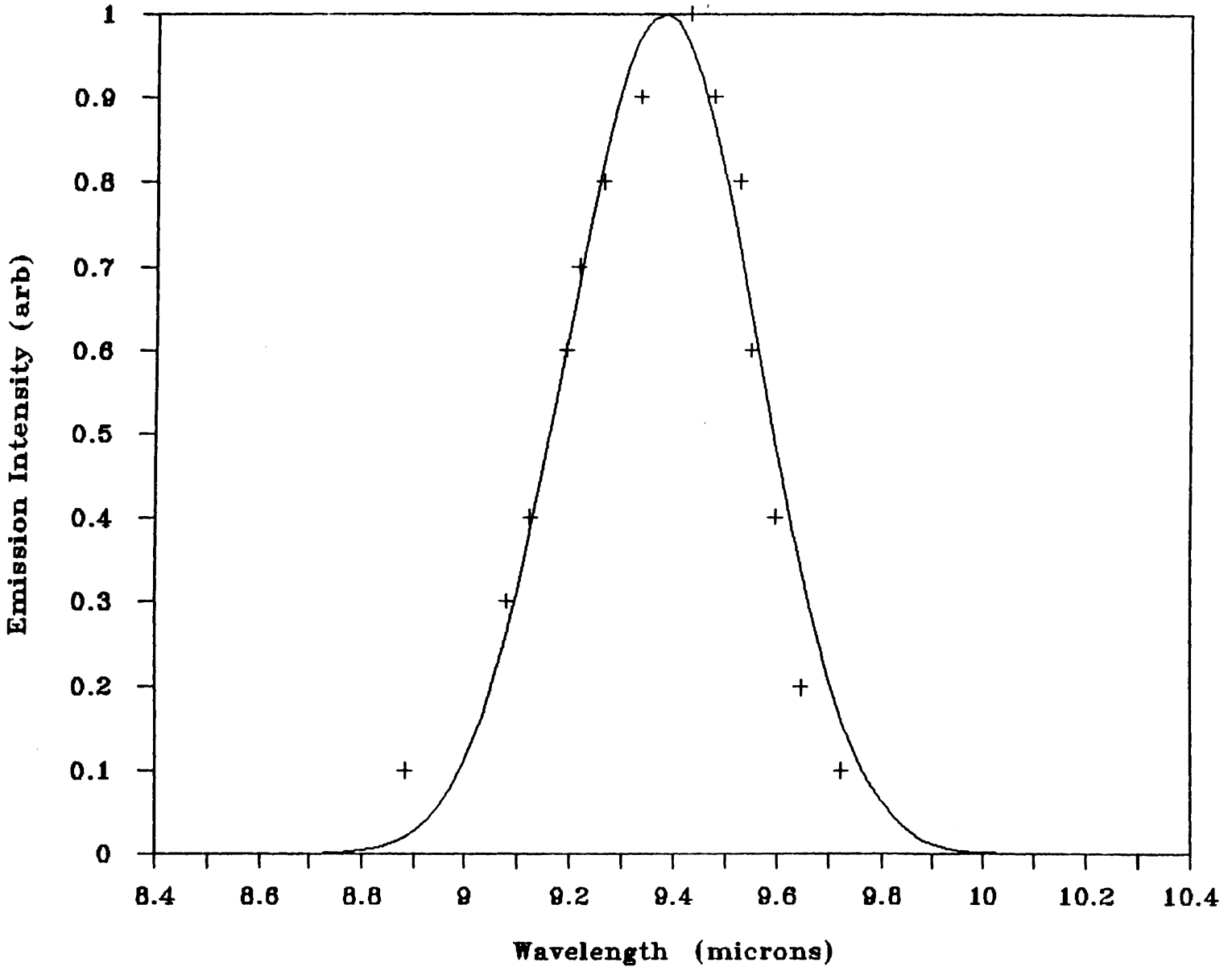
Emission Intensity (arb)
1
0.9
0.8
0.7
0.6
0.5
0.4
0.3
0.2
0.1
0
8.4
8.6
8.8
9
9.2
9.4
9.6
9.8
10
10.2
10.4
Wavelength (microns)

Fig.3–11 Emission spectrum for the 20 μm thick, 20% Sn epilayer with P = 1.6 x 10^{17} cm^{-3} at T = 77K at I = 20 MW cm^{-2} (—— model prediction; + experimental)

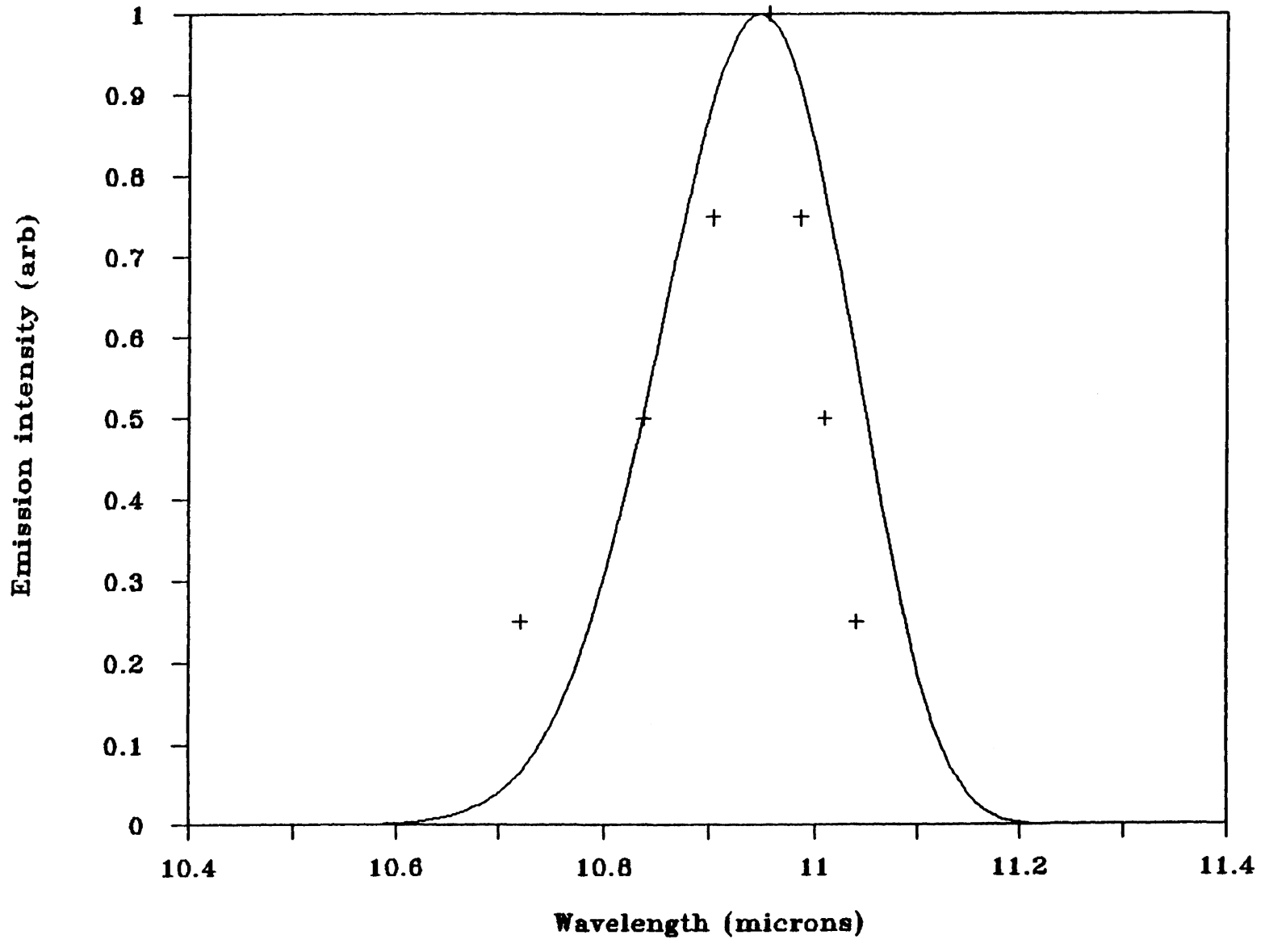
Emission intensity (arb)
1
0.9
0.8
0.7
0.6
0.5
0.4
0.3
0.2
0.1
0
10.4
10.6
10.8
11
11.2
11.4
Wavelength (microns)

Fig.3–12 Emission spectrum for the chemically etched 18 μm thick, 20% Sn epilayer with P = 2.3 x 10^{17} cm^{-3} at T = 77K at I = 20 MW cms^{-2} (—— model prediction; + experimental)

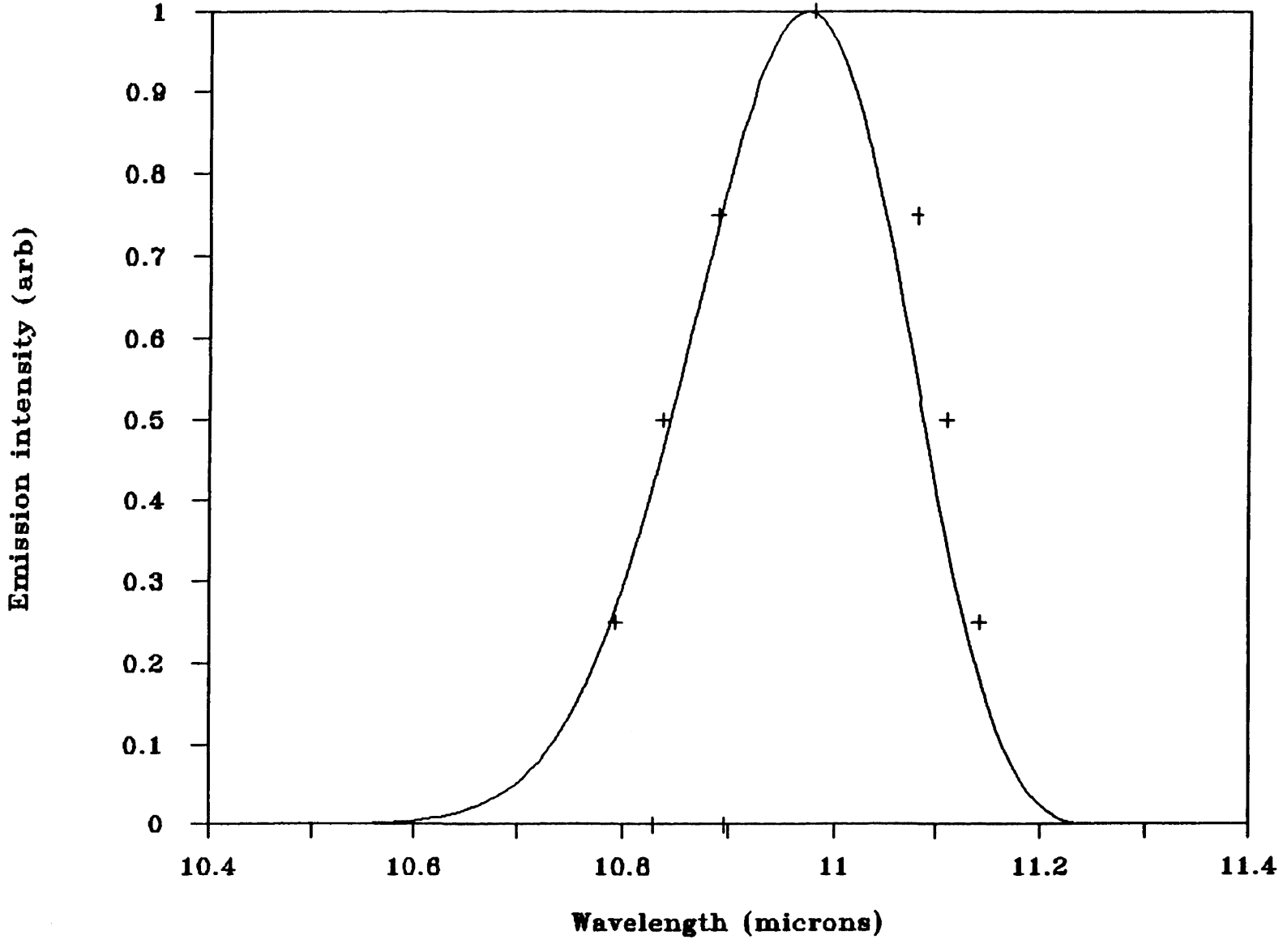
Emission intensity (arb)
1
0.9
0.8
0.7
0.6
0.5
0.4
0.3
0.2
0.1
0
10.4
10.6
10.8
11
11.2
11.4
Wavelength (microns)

region. Hence, the optical field is no longer seeing the optical loss in the entire epilayer and optical gain can be produced in this thick film. Good fits to the measured emission spectra were obtained by assuming a doping density of 4×10^{16} cm^{-3} μm^{-1} in the epilayer. Figs. 3–11 and 3–12 show the model predicted spectra and the measured emission spectra.

To summarize the results of the experiments; single pass optical net gain was measured directly for the first time for $Pb_{1-x}Sn_xTe$ material and the stimulated emission spectra for various samples were also observed.

3.3.3 Comparisons with Theory

According to the model predicted results in section 3.2.4, the mode–gain value is dependent upon both the mode size (equivalent to the epilayer thickness if the layer is homogeneous) and the doping density. Therefore, the epilayer thickness as well as the doping density are to be known so that the model predicted results can be compared with the experimental results. The physical thickness of the epilayer was measured by optical microscope and the doping density was determined by Hall effect at room temperature. Table I summarizes all the measurements of the layer doping density, the measured optical net gain and the predicted mode–gain.

Table I shows that the predicted mode–gain values derived from the experimental conditions agree with the measured optical net gain values to within a 10% accuracy. For the 2.3 and 4 μm thick samples, the measured doping densities at room temperature were about 9.2×10^{17} cm^{-3} and 1.6×10^{18} cm^{-3} respectively.

Table I Comparisons of the Predicted Mode-Gain with the Measured Optical Gain

Sample Structure	Thick-ness (μm)	Doping Density at 300K (cm^{-3})	Measured Optical Gain (cm^{-1})	Assumed Doping at 77K (cm^{-3})	Predicted Mode-Gain (cm^{-1})
$\frac{Pb_{.94}Sn_{.06}Te}{PbSe_{.02}Te_{.98}}$	2	/			
	10	/	100	$4x10^{17}$	100*
$\frac{Pb_{.94}Sn_{.06}Te}{BaF_2}$	5	/			
$\frac{Pb_{.82}Sn_{.18}Te}{BaF_2}$	2.3	$9.2x10^{17}$	370	$6x10^{17}$	340
$\frac{Pb_{.82}Sn_{.18}Te}{BaF_2}$	4	$1.6x10^{18}$	220	$1x10^{18}$	240
$\frac{Pb_{.80}Sn_{.20}Te}{BaF_2}$	20	$4x10^{18}$	/	#	100

* gain number obtained by assuming that the emission was confined within the top layer (2 μm thick of PbSnTe)

\# assumed a doping gradient of $4x10^{16}$ $cm^{-3}\mu m^{-1}$ with a surface doping density of $1.6x10^{17}$ cm^{-3}

From our experience with the Hall effect measurements of $Pb_{1-x}Sn_xTe$ epilayers, the doping density decreases by a factor of about 1.5 in average from room temperature to 77K. Therefore, the doping densities for the 2.3 and 4 μm thick films at 77K are 6×10^{17} cm^{-3} and 1×10^{18} cm^{-3} respectively. The gain numbers obtained from the model were in very good agreement with the measured values.

The next step is to compare the predicted A.S.E. spectrum with the measured emission spectrum. Fig.3–10 presents the predicted spectrum according to the conditions listed in Table I and the measured emission spectrum for the 2.3 μm thick sample. Both the predicted emission peak and the spectral width agree very well with the experimental results. However, the measured spectral shape is more asymmetric than the predicted spectral width. This could be accounted for by the inaccuracy of the band parameters in describing the region of the energy band high above the energy band gap and can be corrected by adjusting the band parameters by about 10 %.

3.4 Discussion and Conclusion

A N_2 laser optically pumped $Pb_{1-x}Sn_xTe$ laser model was presented and the non–homogeneous complex dielectric constant spatial profile was also examined . It was found that the optical field was not confined within the optical gain region but was spread out over the entire epilayer through the approximation obtained by a step index dielectric constant profile model. Good fits to the observed stimulated emission spectra were produced by the model. This can be taken as a further verification that the optical absorption edge shifting effect were indeed induced by the free carrier density, apart from the transmission experiments that were reported in chapter two.

In conclusion, the model predicted results adequately describe the experimental results. The model predicted effects of the re–absorption in the unpumped region was also shown to be present in the experiments. This is seen by comparing the the optical gain number difference for the different thickness samples at the same pump intensity. These results also confirm the doping density effect of the near band gap optical absorption, which modified the mode–gain values greatly in the experiments. Finally, the model relating optical gain and pump intensity was found to be in very good agreement with the experimental results.

CHAPTER 4

DISCUSSION AND CONCLUSIONS

In this thesis, results of an experimental and theoretical study of optical gain and amplified spontaneous emission (A.S.E.) in $Pb_{1-x}Sn_xTe$ thin film waveguides were reported. The optical gain for the same pumping condition was shown to depend dramatically on the doping densities of the films.

The possibility of producing a $Pb_{1-x}Sn_xTe$ laser, using a CO_2 laser as pump source was examined. A model, which was developed to calculate the gain as a function of pump power for films of various doping densities and thicknesses, predicted that such a laser should be readily achievable, needing a pump intensity of only 10^{3} Watts cm^{-2} at temperatures lower than 77K, provided that epilayer doping densities of 10^{17} cm^{-3} or less can be produced. However, doping densities even in nominally undoped layers are generally at least an order of magnitude too high. In some initial attempts to achieve lower doping densities, using a thermal annealing technique, doping densities as low as 2×10^{17} cm^{-3} at 77K have been obtained and significant pump absorption was achieved at 9.52 μm, the 9P(16) line of CO_2 laser, as predicted by the model. Room temperature operation of this laser was also predicted by the same model to be achievable at a pump intensity of about 10^{5} Watts cm^{-2}.

In order to ensure that sufficient pump power will be absorbed by the $Pb_{1-x}Sn_xTe$ film, a laser with adequate pump power and short enough wavelength is needed. A pulsed Nitrogen laser was chosen as the pump source since it has very high pump power, and emits at 0.337 μm, a very short wavelength, at which the

$Pb_{1-x}Sn_xTe$ epilayers have very high optical absorption. A modified version of the CO_2 laser pumping model was also developed for the N_2 laser pumping conditions. This modified model is needed because of the non steady state condition due to the short duration of the laser pulse (300 picoseconds), and the presence of the pumped and unpumped region due to the very high optical absorption at N_2 laser wavelength. It was also shown through a simple waveguide model that the optical field was confined within the epilayer, overlapping both the gain and loss regions. Therefore, the net–gain was calculated by integrating the gain coefficients over the entire epilayer.

According to this model, net–gain numbers of comparable values ($\pm$ 10 %) to the measured optical net gain numbers were obtained. Net–gain values of 370 cm^{-1} and 220 cm^{-1} were measured for two separate samples with film thicknesses of 2.3 and 4 μm respectively. The net–gain, which decreases with the film thickness, is consistent with the model predictions. Good fits to the A.S.E. spectra were also produced by the same model. This is the first time that single pass optical gain in Pb salt material was measured and compared directly with a theoretical model.

According to the results obtained in N_2 laser optical pumping, $Pb_{1-x}Sn_xTe$ is capable of achieving sufficient optical gain to produce laser action by optical pumping. Since significant increase in CO_2 laser pump absorption with films produced by the thermal annealing method has been demonstrated, future experiments using the same method should be attempted to reduce the doping densities of the films.

APPENDIX A

EXTINCTION COEFFICIENT

The complex index of refraction is given by

$$n_c = n_r - in_i \tag{A.1}$$

where n_r is usually referred to as the refractive index, n_i is the extinction coefficient. The velocity of propagation in vacuum, c is related to the complex index of refraction by

$$v = \frac{c}{n_c} \tag{A.2}$$

therefore,

$$\frac{1}{v} = \frac{n_r}{c} - i\frac{n_i}{c} \tag{A.3}$$

For a plane wave, the radiation propagating with an angular frequency ω_0 in the x–direction with a velocity v is given by

$$\xi = \xi_0 \exp\left[i\omega_0(t-x/v) \right] \tag{A.4}$$

substitute (A.3) into (A.4) gives

$$\xi = \xi_0 \exp(i\omega_0 t) \exp(-i\omega_0 n_r x/c) \exp(-\omega_0 n_i x/c) \tag{A.5}$$

Note that the last term in (A.5) is an attenuation factor. The fraction of the incident power available after propagating a distance x through the material is

$$P(x) = P_0 \exp(-2\omega_0 n_i x/c) \tag{A.6}$$

and the absorption coefficient is defined as

$$P(x) = P_0 \exp(-\alpha x) \tag{A.7}$$

therefore,

$$n_i = \frac{\alpha c}{2\omega_0} \tag{A.8}$$

APPENDIX B

DERIVATION OF THE WAVE EQUATION

In a linear isotropic dielectric media, the electric field $\vec{E}$, the electric displacement $\vec{D}$, the magnetic field $\vec{H}$, and the magnetic flux density $\vec{B}$ are related by the following equations

$$\nabla \times \vec{H} = \frac{\partial \vec{D}}{\partial t} \tag{B.1}$$

$$\nabla \times \vec{E} = -\frac{\partial \vec{B}}{\partial t} \tag{B.2}$$

$$\vec{D} = \epsilon \epsilon_0 \vec{E} \tag{B.3}$$

$$\vec{B} = \mu \vec{H} \tag{B.4}$$

where ϵ is the dielectric constant, ϵ_0 is the permittivity in vacuum, μ is the magnetic permeability. In the absence of electric charges, the vector $\vec{D}$ satisfies the relation

$$\nabla \cdot \vec{D} = 0 \tag{B.5}$$

and the magnetic flux density always obeys the relation

$$\nabla \cdot \vec{B} = 0 \tag{B.6}$$

substitue (B.4) into (B.2) and take the curl of the resulting equation

$$\nabla \times (\nabla \times \vec{E}) = -\mu_o \frac{\partial}{\partial t} (\nabla \times \vec{H}) \tag{B.7}$$

We can obtain an equation which only depends on $\vec{E}$ by substituting (B.1) and (B.3) into (B.7)

$$\nabla \times (\nabla \times \vec{E}) + \epsilon\epsilon_o\mu_o \frac{\partial^2 \vec{E}}{\partial t^2} = 0$$

Making use of the following indentity which holds for the cartesian coordinate system

$$\nabla \times (\nabla \times \vec{E}) = \nabla (\nabla \cdot \vec{E}) - \nabla^2 \vec{E}$$

with the help of (B.3) and (B.5), we obtain

$$\nabla^2\vec{E} + \nabla\left(\vec{E}\cdot\frac{\nabla\epsilon}{\epsilon}\right) = \epsilon\epsilon_0\mu_0\frac{\partial^2\vec{E}}{\partial^2 t} \tag{B.8}$$

Since a step profile approximation to the spatial distribution of the dielectric constant within the film was chosen, ϵ is a constant in space over each of the two regions, the gradient of ϵ vanishes and (B.8) in each region takes the form of the wave equation

$$\nabla^2\vec{E} = \frac{\epsilon}{c^2}\frac{\partial^2\vec{E}}{\partial t^2} \tag{B.9}$$

where $c = (\epsilon_0\mu_0)^{-1/2}$ is the velocity of light in vacuum.

Fig.1–2 shows the geometry of the $Pb_{1-x}Sn_xTe$ epilayer. A few simplifying assumptions are possible at this point. First, because the focused laser beam diameter is larger than the sample width, the central area is uniformly pumped. It follows that the optical parameters are not dependent on the spatial variation y. Moreover, since the variation in dielectric constant along the x–axis occur over a much shorter distance than along the cavity axis z (the thickness of the active region is much smaller than the cavity length), the transverse modes should not be affected by the modal distribution along the cavity axis much. Assuming that the modal distribution along the z axis takes the form of a standing wave, we write the trial solution as follows

$$\vec{E}(x,z,t) = A(x,t)\sin(\pi\frac{Nz}{l})\,e^{i\omega t}\,\vec{a}_y$$

where A is the field distribution along the x–axis, N is the mode order along the z–axis, l is the cavity length and ω is the light frequency and $\vec{a}_y$ is the unit vector along the y direction.

Substituting the above expression for the field into the wave equation (B.9), we obtain

$$\frac{\partial^2 A}{\partial x^2} - \beta^2 A = \frac{\epsilon}{c^2}\left(\frac{\partial^2 A}{\partial t^2} + 2i\omega\frac{\partial A}{\partial t} - \omega_o{}^2 A\right) \qquad \text{(B.10)}$$

where β is the propagation constant along the cavity axis. On the time scale of the light freqency, the other time–dependent variations of the optical parameters are much slower. This justifies the use of the condition for a steady state

$$\frac{\partial^2 A}{\partial x^2} = \left(\beta^2 - \epsilon\frac{\omega_o{}^2}{c^2}\right)A \qquad \text{(B.11)}$$

REFERENCES

1. H. Preier, "Recent advances in lead–chalcogenide diode lasers", Appl. Phys., 20, p.189–206 (1979)
2. M. P. Gomez, D. A. Stevenson, and R. A. Huggins, "Self–Diffusion of Pb and Te in Lead Telluride", J. Phys. Chem. Solids, 32, p.335 (1971)
3. J. I. Pankove, "Optical Processes in Semiconductors", London, Constable and Company Ltd., p. 249 – 252 (1971)
4. K. L. Shaklee, "Optical gain in semiconductors", Journal. of Luminescence, 7,p.284–309 (1973)
5. A. Lopez–Otero, "Hot Wall Epitaxy", Thin Solid Films, V.49, p. 5, (1978)
6. W. W. Anderson, "Gain–Frequency–Current Relation for $Pb_{1-x}Sn_xTe$ Double Heterostructure Lasers", IEEE J.Quantum Electronics, V. Q.E.–13, p.532–543, (1977)
7. R. Grisar, W. J. Riedel, and H. G. Preier, IEEE J. Quantum Electron., QE–17, p.586 (1981)
8. C. R. Hewes, M. S. Adler, and S. D. Senturia, "Nuclear –magnetic resurce studies in PbTe and $Pb_{1-x}Sn_xTe$: An experimental determination of k p band parameters and magnetic hyperfine constants", Phys. Rev. B, V–7, p.5195–5211 (1973)
9. W. W. Anderson, "Absorption Constant of $Pb_{1-x}Sn_xTe$ and $Hg_{1-x}Cd_xTe$ Alloys". Infrared Phys., V.20, P.363–372, (1980)
10. J. O. Dimmock, "k p theory for the conduction and valance bands of

$Pb_{1-x}Sn_xTe$ and $Pb_{1-x}Sn_xSe$ alloys", in The Physics of Semimetals and Narrow–Gap Semiconductors, D. L. Carter and R. T. Bates, Eds. Oxford : Pergamom, p.319–330 (1971)

11. J. S. Blakemore, "Carrier Concentrations and Fermi levels in Semicondictors", Electrical Communications, p.131–153, (1952)

12. G. Lasher and F. Stern, "Spontaneous and Stimulated Radiation in Semiconducctors",Phys. Rev., V.133, No.2a, p.A533–A563, (1963)

13. E. Burstein, "Anomalous optical absorption limit in InSb", Phys. Rev., V.93, p.632–633 (1954)

14. T. S. Moss, "The interpretation of the properties of indium antimonide", Proc. Phys. Soc. B, V.67, p.755–782 (1954)

15. M. Oron, A. Zussman and A. Katzir, "Dielectric Constant and Optical Confinement in Homostructure PbSnTe Diode Lasers", Infrared Phys., V.22, p.317–322, (1982)

16. V. Gopal, "Energy Gap–Refractive Index Interrelation", Infrared Phys., V.22, p.255–257, (1982)

17. W. Lo, D. L. Partin, "Overview of Tunable Diode Laser Technology", Proc. SPEI, V.461, p.5 (1984)

18. I. Melngailis, T. C. Harman, In Semiconductors and Semimetals, V.5, ed. by R. K. Willardson and A. C. Beer, Academic Press, New York, p.111 (1970)

19. R. Roseman, A. Katzir, "Lifetime Calculations for Auger Recombination in Lead–Tin–Telluride", IEEE J.Q.E., V.18, p.814–817, (1982)

20. C. A. Klein, Appl. Optics, V.5, p.1922 (1966)

21. Y. Yang, B. K. Garside and P. E. Jessop, "Heterolayer lead–salt diode laser", Can. J. Phys., V.65, p.999–1002 (1987)

22. J. F. Young, and H. M. van Driel, "Ambipolar diffusion of high–density electrons and holes in Ge, Si, and GaAs: Many–body effects", Phys. Rev. B, V.26, p.2146–2158 (1982)